AD-A174 673 TEMPERATURE COMPENSATION OF SURFACE TRANSVERSE WAVES FOR STABLE OSCILLATO (U) STANFORD UNIV CA EDWARD L GINZTON LAB OF PHYSICS B A AULD ET AL OCT 86 1/1

UNCLASSIFIED RADC-TR-86-168 F19628-83-K-0011 F/G 20/1 NL

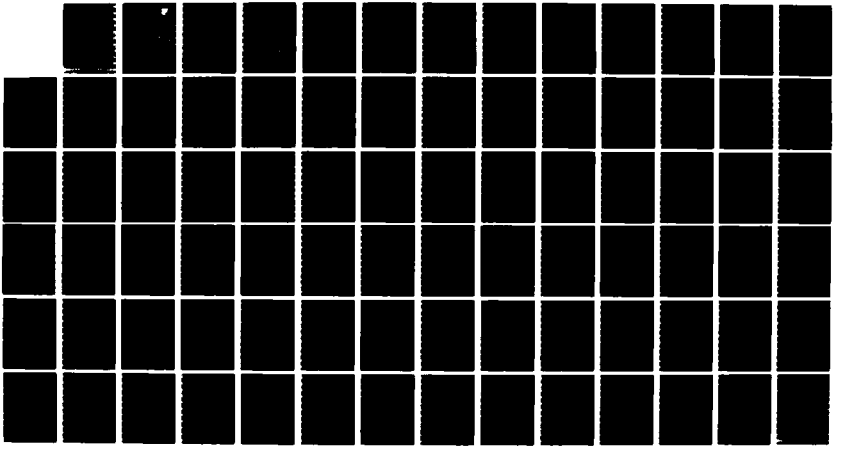

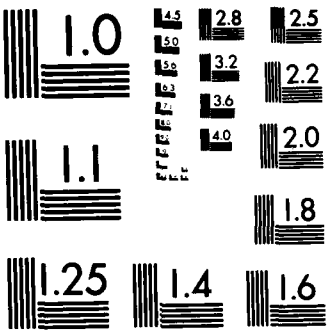

MICROCOPY RESOLUTION TEST CHART
NATIONAL BUREAU OF STANDARDS-1963-A

(12)

RADC-TR-86-168
Final Technical Report
October 1986

TEMPERATURE COMPENSATION OF SURFACE TRANSVERSE WAVES FOR STABLE OSCILLATOR APPLICATIONS

Stanford University

B. A. Auld and D. F. Thompson

APPROVED FOR PUBLIC RELEASE; DISTRIBUTION UNLIMITED

ROME AIR DEVELOPMENT CENTER
Air Force Systems Command
Griffiss Air Force Base, NY 13441-5700

AD-A174673

UNCLASSIFIED
SECURITY CLASSIFICATION OF THIS PAGE

REPORT DOCUMENTATION PAGE

1a. REPORT SECURITY CLASSIFICATION UNCLASSIFIED	1b. RESTRICTIVE MARKINGS N/A
2a. SECURITY CLASSIFICATION AUTHORITY N/A	3. DISTRIBUTION/AVAILABILITY OF REPORT Approved for public release; distribution unlimited.
2b. DECLASSIFICATION/DOWNGRADING SCHEDULE N/A	
4. PERFORMING ORGANIZATION REPORT NUMBER(S) N/A	5. MONITORING ORGANIZATION REPORT NUMBER(S) RADC-TR-86-168
6a. NAME OF PERFORMING ORGANIZATION Stanford University 6b. OFFICE SYMBOL (If applicable)	7a. NAME OF MONITORING ORGANIZATION Rome Air Development Center (EEAC)
6c. ADDRESS (City, State, and ZIP Code) Edward L. Ginzton Laboratory Stanford CA 94305	7b. ADDRESS (City, State, and ZIP Code) Hanscom AFB MA 01731-5000
8a. NAME OF FUNDING/SPONSORING ORGANIZATION Rome Air Development Center 8b. OFFICE SYMBOL (If applicable) EEAC	9. PROCUREMENT INSTRUMENT IDENTIFICATION NUMBER F19628-83-K-0011
8c. ADDRESS (City, State, and ZIP Code) Hanscom AFB MA 01731-5000	10. SOURCE OF FUNDING NUMBERS PROGRAM ELEMENT NO: 61102F; PROJECT NO: 2305; TASK NO: J5; WORK UNIT ACCESSION NO: 32

11. TITLE (Include Security Classification)
TEMPERATURE COMPENSATION OF SURFACE TRANSVERSE WAVES FOR STABLE OSCILLATOR APPLICATIONS

12. PERSONAL AUTHOR(S)
B. A. Auld, D. F. Thompson

13a. TYPE OF REPORT	13b. TIME COVERED	14. DATE OF REPORT (Year, Month, Day)	15. PAGE COUNT
Final	FROM Mar 83 TO Dec 85	October 1986	86

16. SUPPLEMENTARY NOTATION
N/A

17. COSATI CODES			18. SUBJECT TERMS (Continue on reverse if necessary and identify by block number)
FIELD	GROUP	SUB-GROUP	Surface Transverse Waves (STW); Delay Lines; Surface Acoustic Waves (SAW); Resonators; Temperature Compensation; Gratings (See Reverse)
20	14		
21	02		

19. ABSTRACT (Continue on reverse if necessary and identify by block number)

The purpose of this research is to further develop theory describing surface-type acoustic wave resonator and delay line temperature compensation in the high coupling materials such as lithium niobate and lithium tantalate. Several models are developed to predict the temperature behavior of acoustic wave propagation beneath periodic corrugated surface gratings. The grating types considered include grooves, mass loading strips, conducting strips, and combinations thereof. Temperature and stress characteristics of these acoustic waves are determined not only by the crystalline material properties, mass and stiffness, but also by the structure and dimensions of the surface grating. It is this property that allows the use of a surface grating as an effective means for temperature compensating surface acoustic wave resonators and delay lines of this type. Grating dimensions required to temperature compensate surface transverse wave (STW) propagation normal to the X-axis on rotated Y-cuts of quartz, lithium niobate and lithium tantalate are presented. In this configuration the STW is, however, nonpiezoelectrically active for the lithium materials

20. DISTRIBUTION/AVAILABILITY OF ABSTRACT ☐ UNCLASSIFIED/UNLIMITED ☒ SAME AS RPT ☐ DTIC USERS	21. ABSTRACT SECURITY CLASSIFICATION UNCLASSIFIED
22a. NAME OF RESPONSIBLE NDIVIDUAL Paul H. Carr	22b. TELEPHONE (Include Area Code) (617) 861-377 22c. OFFICE SYMBOL RADC (EEAC)

DD FORM 1473, 84 MAR 83 APR edition may be used until exhausted. All other editions are obsolete.

SECURITY CLASSIFICATION OF THIS PAGE
UNCLASSIFIED

and an external transducer is required. Grating dimensions required to temperature compensate the Rayleigh-type surface acoustic wave propagation normal to the X-axis on rotated Y-cuts of lithium niobate and lithium tantalate, which are piezoelectrically active, are also presented along with a proposed experimental device. For delay line applications, the operation frequency is in the passband of the grating structure; for resonator applications two gratings are required--a passband grating for the standing wave region and a stopband grating for the reflecting regions. In addition, a software package is developed to calculate the grating dimensions needed to slow a general acoustic wave to prespecified velocity. This program allows for the investigation of arbitrary crystal orientations including trapped leaky wave orientations on the higher coupling materials which have yet to be considered for their temperature properties.

Item 18. SUBJECT TERMS (Continued)

Lithium Tantalate
Lithium Niobate
Surface Skimming Bulk Waves (SBAW)
Leaky Surface Waves
Static Strain
Nonlinear Strain
Temperature Coefficient of Delay (TCD)
Doubly Rotated
Triclinic

TABLE OF CONTENTS

I. INTRODUCTION

The temperature stability of surface acoustic wave resonator and delay line devices has long been a major concern for system designers. When designing a high frequency SAW resonator, temperature-compensated crystal cuts are selected to aid in maintaining oscillator stability. In many materials, lithium niobate and lithium tantalate, for example, these temperature-compensated crystal cuts may be nonexistent. Even in those materials where the temperature-compensated cuts do exist, quartz, for example, they may not be optimum with respect to other properties—for example, insertion loss, piezoelectric coupling, or wave velocity. In order to provide increased freedom in the design of these devices, this report summarizes the results of an investigation of the temperature compensation of surface transverse waves for stable oscillator applications.

II. TEMPERATURE COMPENSATED SURFACE TRANSVERSE WAVES

(a) Background

It has been previously shown that horizontally-polarized shear surface waves (STW) can exist on a semi-infinite substrate with a periodic corrugation or grating on the surface[1,2]. This phenomenon differs from Rayleigh wave propagation, on structures currently used in SAW resonator applications, by the fact that the shear surface wave does not exist in the absence of the grating. For a smooth semi-infinite isotropic substrate a shear surface skimming bulk wave (SSBW) does satisfy the stress-free boundary conditions. This SSBW solution can also exist for certain orientations of anisotropic substrates. Placing a corrugation or grating on the surface slows down this SSBW in a manner entirely analogous to that in the corresponding electromagnetic problem,[3,4] and thereby converts it into a shear surface wave—a Surface Transverse Wave (STW). A SSBW, and thus a STW, can exist on trigonal crystal plates if propagation is normal to the X-axis. The basic wave theory for this geometry has already been developed neglecting piezoelectricity.[5,6]

The surface transverse wave (STW) has several inherent advantages over SAW: (1) Higher acoustic velocity, leading to larger IDT periodicities at the same frequency; (2)

Low propagation loss; and (3) Temperature characteristics that are dependent on the grating structure used to trap the wave energy on the surface, as well as on the crystal orientation. By properly choosing the grating height, this third advantage allows one to predict temperature compensation in quartz for STW propagating normal to the X-axis for almost all rotated Y-cuts. Compensation can also be achieved for several rotated Y-cut angles of lithium niobate and lithium tantalate crystal plates.

This grating temperature compensation effect can be explained by referring to the dispersion curve in Fig. 1. In the absence of the grating, the dispersion curve is the (SSBW) line. When the temperature is changed, the slope of this line changes because of changes in density and elastic constants. In the presence of the grating a stop-band appears ($\delta\omega$), with a width that is a function of the crystal stiffness constants, the crystal density, and the grating dimensions. As the temperature changes, the width of this stop band changes. To achieve temperature compensation, the width of the stop band must change with temperature in a way that compensates for the changing slope of the SSBW line, so that an operating point on the STW curve (ω_r) remains stationary. This can be achieved in many cases by selecting appropriate grating dimensions for a given crystal type and orientation.

It has been found that the theoretical temperature compensation achieved for STW propagation normal to the X-axis on rotated Y-cut quartz is comparable to, and for some orientations surpasses that for, the AT cut surface skimming bulk waves. Temperature compensation of STW propagation normal to the X-axis on rotated Y-cut lithium niobate and lithium tantalate crystal plates can also be achieved with deep gratings. However, these crystal orientations are unfortunately not piezoelectrically active in the cases of niobate and tantalate.

The STW analysis referred to above considered propagation on corrugated surfaces of rotated Y-cut trigonal class crystals with grating dimensions corresponding to the cavity region of Fig. 2, where the STW is in a pass-band. The method used was to apply Floquet's Theorem, which gives the general form of the characteristic wave solutions, separately to the semi-infinite substrate and to the grating. Application of appropriate boundary

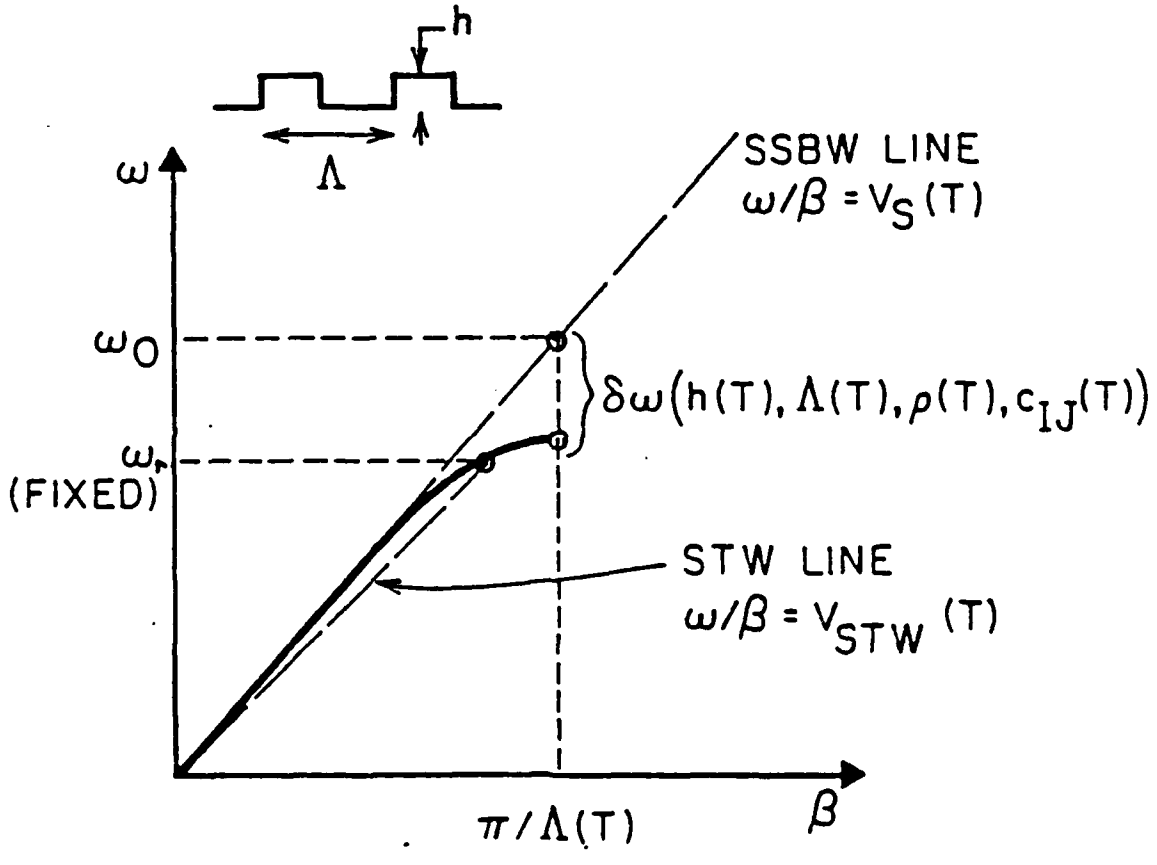

FIGURE 1

Grating termperature compensation mechanism for STW. The effect of temperature on the SSBW line is balanced by changes in the stopband width and position on the β axis.

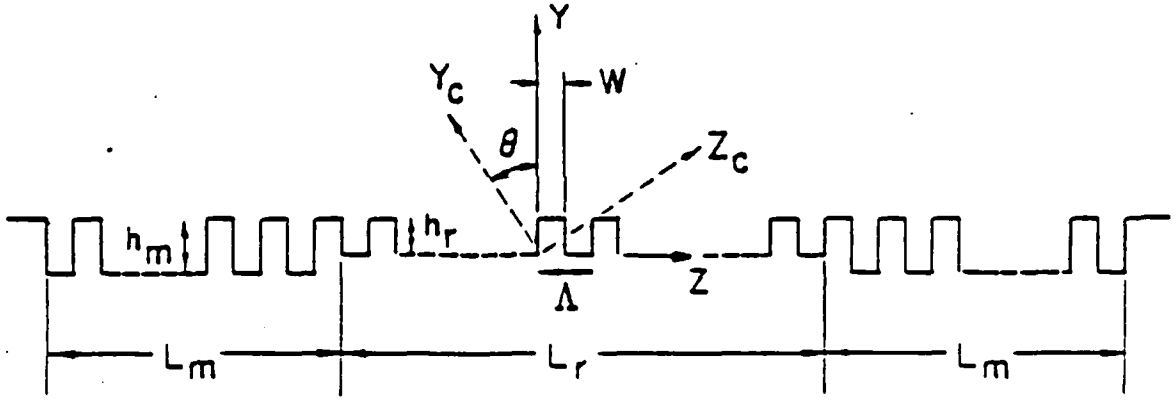

FIGURE 2

STW grating resonator structure on a rotated Y-cut quartz plate with grating tooth width $W = \Lambda/2$.

conditions at the grating-substrate interface then gives the dispersion relation and the relative amplitudes of the various space harmonics. In applying the boundary conditions a shallow grating was assumed, and the stress at the bottom of a tooth was calculated using the Datta-Hunsinger Perturbation Formula.[7] A review of this STW theory follows, along with a detailed analysis of the STW temperature characteristics.

(b) Surface Transverse Wave (STW) Theory for Grooved Gratings

Starting from the general acoustic field equations one can derive the following differential acoustic wave equation governing horizontal shear wave propagation normal to the X-axis in trigonal rotated Y-cut crystal substrates.

$$c_{66}\frac{\partial^2 v_x}{\partial y^2} + 2c_{56}\frac{\partial^2 v_x}{\partial y \partial z} + c_{55}\frac{\partial^2 v_x}{\partial z^2} = \rho\frac{\partial^2 v_x}{\partial t^2} \tag{1}$$

where

v_x	is the particle displacement velocity
c_{ij}	are rotated stiffness constants
ρ	is the density of the trigonal crystal
$x, y,$ and z	are the space coordinates
t	is the time coordinate

A solution based on Floquet theory consisting of an infinite sum of space harmonics is assumed in the substrate ($Y < 0$ in Fig. 2).

$$v_x = \sum_{n=-\infty}^{\infty} a_n e^{\alpha_n y} e^{-i\beta_n z} e^{i\omega t}$$
$$\beta_n = \beta_o + \frac{2\pi n}{\Lambda} \tag{2}$$

where

a_n	is the nth space harmonic amplitude
β_n	is the space harmonic propagation constant
α_n	is the lateral attenuation constant into the substrate
ω	is the steady state angular frequency
Λ	is the grating period

Each space harmonic solution is substituted into Eq. 1, resulting in the following relation for the nth space harmonic lateral attenuation constant

$$\alpha_n = \left[\frac{c_{eff}}{c_{66}}\beta_n^2 - \frac{\rho\omega^2}{c_{66}}\right]^{1/2} + \frac{ic_{56}\beta_n}{c_{66}} \tag{3}$$

where

$$c_{eff} = \frac{c_{55}c_{66} - c_{56}^2}{c_{66}}$$

The amplitudes of the space harmonics a_n's which make up the acoustic wave (Eq. 2) must be selected so as to match the periodic boundary stresses imposed by the surface grating over the entire surface. Because of the periodic nature of this structure, it is a necessary and sufficient condition for the space harmonic amplitudes to match the surface boundary condition over just one period. Thus only the region of a single period need be considered. The tangential stress imposed by the tooth of the grooved grating is given by the following Datta-Hunsinger interface stress relation[7]

$$T_{xy}^s = j\omega\rho' h v_x - h\frac{\partial T'_{xz}}{\partial z} \tag{4}$$

where

T_{xy}^s is the stress in the crystal at the interface $Y = 0$
v_x is the particle displacement, which is the same in the tooth as in the substrate because of the continuity of displacement boundary condition at $Y = 0$
T'_{xz} is the stress in the grooved tooth
h is the height of the tooth
ρ' the density of the tooth
ω is the angular frequency as stated above

In the case of the grooved grating the density ρ' and the stress T'_{xz} are the same as those in the substrate. This is not true in the case of metal strip mass loading, which will be considered later. This surface stress must equal the acoustic field stress in the substrate at $Y = 0$ in Fig. 2. The acoustic field stress in the substrate can be expressed in terms of the displacement velocity and is

$$T_{xy} = \frac{c_{56}}{i\omega}\frac{\partial v_x}{\partial z} + \frac{c_{66}}{i\omega}\frac{\partial v_x}{\partial y} \tag{5}$$

To obtain the a_n's in Eq. 2 the boundary stress at the surface of the substrate, Eq. 4 is set equal to the boundary stress under the grating Eq. 5. This is converted to a set of linear algebraic equations for the a_n's by using the orthogonality of the different

space harmonics. This is done by multiplying each side of the condition equation by the complex conjugate of the qth space harmonic term $\exp[\beta_q z]$, and then integrating over a single period from $Z = 0$ to $Z = \Lambda$. If Eq. 3 is used to eliminate the lateral attenuation constants α_n, the following infinite set of linear equations is obtained[5]

$$\left[c_{eff}\beta_q^2 - \rho\omega^2\right]^{1/2} a_q = \sum_n a_n K_{nq} \tag{6}$$

where

$$q = \ldots -2, -1, 0, 1, 2 \ldots$$

$$c_{eff} = \frac{c_{55}c_{66} - c_{56}^2}{c_{66}}$$

$$k_{nq} = \frac{h}{\Lambda}\frac{1}{\sqrt{c_{66}}}\int_0^{\Lambda/2}\left[-\omega^2\rho - \left\{-i\beta_n c_{eff} \pm c_{56}\sqrt{\frac{c_{eff}}{c_{66}}\beta_n^2 - \frac{\rho\omega^2}{c_{66}}}\right\}\right.$$
$$\left.\cdot\left(-i\beta_n + \delta(z) - \delta(z - \frac{\Lambda}{2})\right)\right]e^{-i(\beta_n - \beta_q)z}$$

The characteristic determinant of this set of equations defines the dispersion relation ($\omega = f(\beta_o)$) for the STW.

When there is no grating ($h = 0$), the right-hand side of Eq. 6 is equal to zero and the following dispersion relation is obtained.

$$\frac{\omega^2}{\beta_q^2} = \frac{c_{eff}}{\rho} = V_s^2$$
$$\beta_q = \beta_0 + \frac{2\pi q}{\Lambda} \tag{7}$$

where V_s is the SSBW velocity. This is the SSBW dispersion relation, but periodically replicated for each value of q. This is exactly what is expected, since the SSBW is the wave solution in the absence of the grating.

The top of Fig. 3 shows a graph of Eq. 7 for $q = 0$. The bottom shows the SSBW dispersion curves repeated for each space harmonic. (Note that all of the curves are plotted against the same abscissa β_0.) The points where pairs of curves cross correspond to a resonant point between the two space harmonics comprising the two crossing curves. For example, the point where the forward-going 0th space harmonic and the backward-going

- SINGLE SPACE HARMONIC RESPONSE

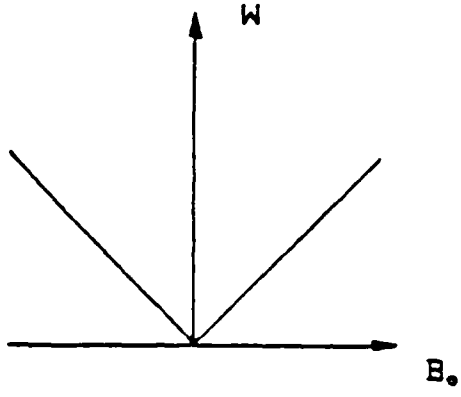

- MULTIPLE SPACE HARMONIC RESPONSE WITH COUPLING BETWEEN ADJACENT HARMONICS

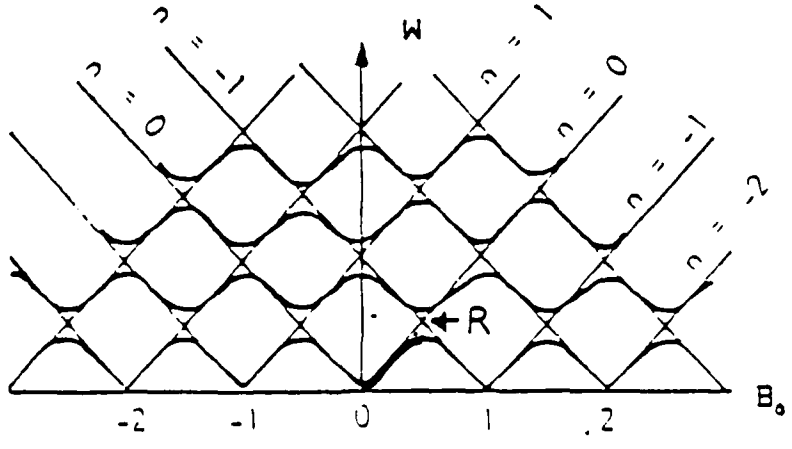

FIGURE 3

Space harmonic dispersion curves.

-1th space harmonic lines intersect (R in Fig. 3) corresponds to the resonance point $\beta_0 = \pi/\Lambda$ and $\omega = V_s\pi/\Lambda$. At this point the left hand side of (Eq. 6), is equal to zero for $q = 0$ and $q = -1$ and non zero for all other values of q. Thus, the magnitude of the 0th and -1th space harmonics have to be much much greater than any other space harmonics in order to maintain the equality of the space harmonic equation. The amplitudes of the space harmonics, of course, cannot become infinite. Solution of Eq. 6 shows that a coupling between the resonant harmonics results in a bending of the dispersion curves away from the resonant point noted. This creates a prohibited frequency band or "stop band" where the STW will not propagate, as shown in the lower part of Fig. 3.

If the surface height h of the grating is small and the analysis is limited to only those values of ω and β_0 near a resonant point, then the two resonant space harmonics are the only non-negligible space harmonic terms. Keeping only the 0th and -1th space harmonics terms reduces the infinite set of equations Eq. 6 to the following coupled linear equations.

$$\begin{aligned} [c_{eff}\beta_{-1} - \rho\omega^2]^{1/2} a_{-1} &= K_{0-1} a_0 \\ [c_{eff}\beta_0 - \rho\omega^2]^{1/2} a_0 &= K_{-10} a_{-1} \end{aligned} \tag{8}$$

where $K_{0,-1} = K^*_{-1,0} = (2\pi\rho V_s^2/\Lambda c_{66})(h/\Lambda)^2$.
These equations are analogous to the well-known (coupled wave theory) used to describe SAW propagation is similar structures.[8]

To calculate the STW dispersion curves from these coupled wave equations, a small frequency perturbation $\delta\omega$, and a small propagation constant perturbation $\delta\beta$ are assumed relative to the 0th and -1th space harmonic resonant point at R in Fig. 3. This leads to the coupled wave dispersion relation found by Renard[5]

$$\delta\beta^2 = (\delta\omega/V_s)^2 - K^2$$

where the surface skimming bulk wave (SSBW) velocity is

$$V_s^2 = (c_{55}c_{66} - c_{56}^2)/\rho c_{66} = c_{eff}/\rho \tag{9}$$

the space harmonic coupling constant is

$$K = \frac{2(\pi)\rho V_s^2}{\Lambda c_{66}} (h/\Lambda)^2$$

and

h is the height of the grating

Λ is the period of the grating

ρ is the density of the crystal

c_{xx} are the crystal stiffness constants

Using the above near-resonance approximation the analytical expression for the velocity of pure STW propagation normal to the X-axis on rotated Y-cut trigonal crystals is

$$V_{stw} = \frac{V_s \omega}{\omega_0 - [(\omega_0 - \omega)^2 - (V_s K)^2]^{1/2}} \tag{10}$$

where the Bragg, or center stop-band, frequency (corresponding to the resonance point R in the figure) is

$$\omega_0 = \pi V_s / \Lambda$$

and the STW operating frequency is ω.

In the low-frequency pass-band of the grating (the heavy line in Fig. 3) the velocity in Eq. 10 must be pure real. From the equation, this obviously requires that

$$(\omega_0 - \omega)^2 > (V_s K)^2 \tag{11}$$

Note that the lower and upper edges of the stop-band are defined by an equality sign in Eq. 11. Since the temperature and rotation angle dependence of V_s, ω_0, and K can be obtained from the temperature dependence of the material constants and grating dimensions, the temperature dependence of the STW velocity can thus be calculated. Knowing the temperature characteristics of the STW velocity, a grating can be selected to temperature compensate the surface wave at room temperature, for crystal cuts at different rotation angles. This will we be presented for both grooved grating and mass loading grating structures in the following sections.

(c) Temperature Compensation of Grooved Grating STW's

The three quantities normally used as a measure of temperature stability in SAW devices are the temperature coefficient of delay (TCD), the fractional time delay change $\Delta t/t$, and the fractional frequency change $\Delta F/F$. In this investigation of the temperature

characteristics of STW the TCD is used to aid in the selection of the grating height, and the fractional frequency change $\Delta F/F$ is used to compare the frequency stability of the various materials and compensation methods. The TCD is defined as[9]

$$\mathrm{TCD} = \alpha - (1/V_{stw})\frac{dV_{stw}}{dT} \tag{12}$$

where V_{stw} is the STW velocity and α is the expansion coefficient in the direction of propagation. To better facilitate the prediction of a grating height that achieves a zero TCD crossing at room temperature, a scheme for relating the TCD curves to the crystal rotation angle was developed, with the grating dimensions and operating frequency as parameters. If only small changes with temperature are considered, and higher order terms are neglected whenever possible, the TCD at frequency ω_r in Fig. 1 can be approximated as

$$\mathrm{TCD} = \frac{H[2(V_{stc} - \Lambda_{tc}) - c_{66tc} + 2h_{tc} + \rho_{tc}] - J[V_{stc} - \Lambda_{tc}]}{F_0 - F_0^2} \tag{13}$$

where

$H =$ $4(h/\Lambda)^4(c_{eff}/c_{66})^2$

$J =$ $\omega/\omega_0 - (\omega/\omega_0)^2$

$F_0 =$ $[(1 - \omega/\omega_0)^2 - H]^{1/2}$

V_{stc} and c_{66tc} are the surface skimming wave velocity and 66 stiffness temperature coefficients in the rotated coordinates;

Λ_{tc} and h_{tc} are the linear expansion coefficients for the period and height in the rotated coordinates;

ρ_{tc} is the temperature coefficient of density of the crystal

This expression can be evaluated for the temperature dependence of the TCD, since the temperature coefficients for c_{66}, h and Λ are known experimentally.[10,11] The skimming bulk wave velocity temperature coefficient is calculated (using Eq. 9) to be

$$V_{stc} = \frac{c_{55}c_{55tc} - (2c_{56tc} - c_{66tc})c_{56}^2/c_{66}}{2c_{eff}} - \rho_{tc}/2 \tag{14}$$

This equation for the surface skimming bulk wave velocity temperature coefficient was checked by substituting the stiffness constants for quartz[11] and comparing with published curves for the SSBW temperature coefficient.[12] An exact match was found.

Setting the TCD equation Eq. 13 equal to zero gives a condition on the frequency ω_r in Fig. 1, the crystal rotation angle θ in Fig. 2, and the grating dimensions required to achieve a TCD zero crossing. This condition is

$$J = HA$$

where J and H are defined by Eq. 13 and A (the compensation factor) is

$$A = \left[2 + \left(\frac{2h_{tc} + \rho_{tc} - c_{\theta\theta tc}}{V_{stc} - \Lambda_{tc}}\right)\right] \tag{15}$$

The compensation factor is a measure of the grating height required for temperature compensation. The greater the compensation factor, the greater the height of the grating required to achieve zero TCD. Since J is positive, it is clear from Eq. 14 that only a rotation angle with a positive compensation factor A can be used to achieve temperature compensation with a grating.

Plots of the compensation factor A vs. Y-cut rotation angle are given for quartz. lithium niobate and lithium tantalate in Figs. 4, 5, 6. Because A for quartz is positive. for almost all the Y-cut angles, the STW can be temperature compensated at any of these angles by properly selecting the grating dimensions. The compensation factor goes to zero at an angle of -50° and again at an angle of 36°. At these angles the grating height for compensation is zero because these orientations, which correspond to the SSBW AT and BT cuts, are already temperature compensated in the absence of the grating. Using this theory, we are able to select grating dimensions that temperature compensate STW propagating normal to the X-axis on rotated Y-cut quartz at essentially all rotation angles. We have selected a few of the better known orientations for quartz and compared their temperature compensating properties to those of the SSBW AT and BT cuts in the following section.

This result has applications in many areas where temperature behavior is of major concern. For example, in reference 44 the temperature characteristics of acoustic filters are used to compensate for temperature changes in the timing-loop electronics of undersea fiber transmission systems. Presently, the temperature characteristics of these filters are

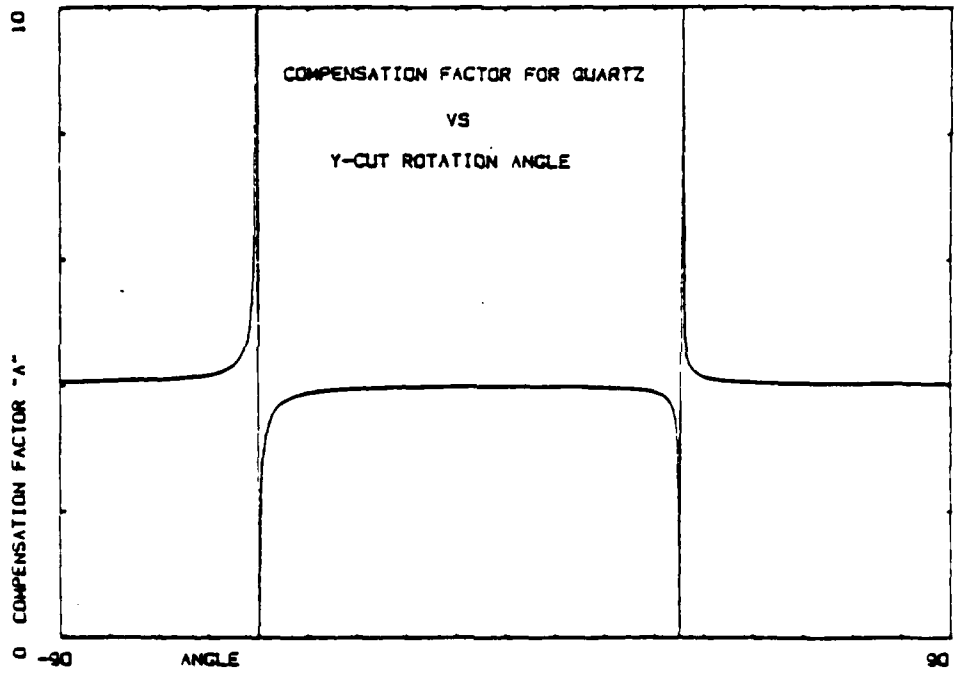

FIGURE 4

Compensation factor A (Eq. 15) versus Y-cut rotation angle for quartz. Grating compensation is possible only for A greater than zero (-90° to -50°, -49° to 35°, 35° to 90°).

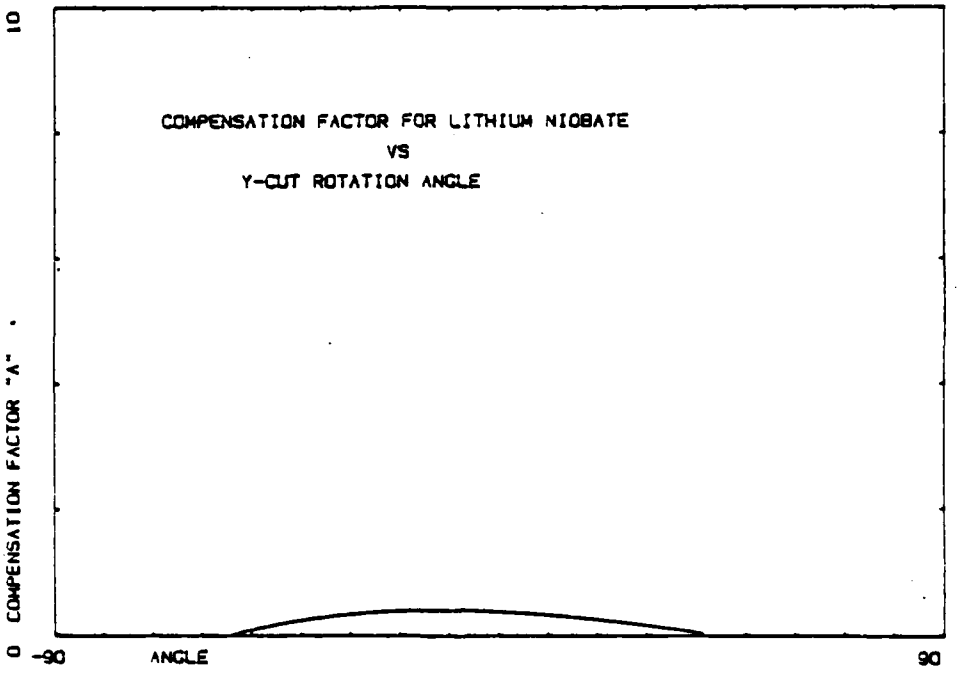

FIGURE 5

As In Fig. 4, for lithium niobate (-54° to 41°).

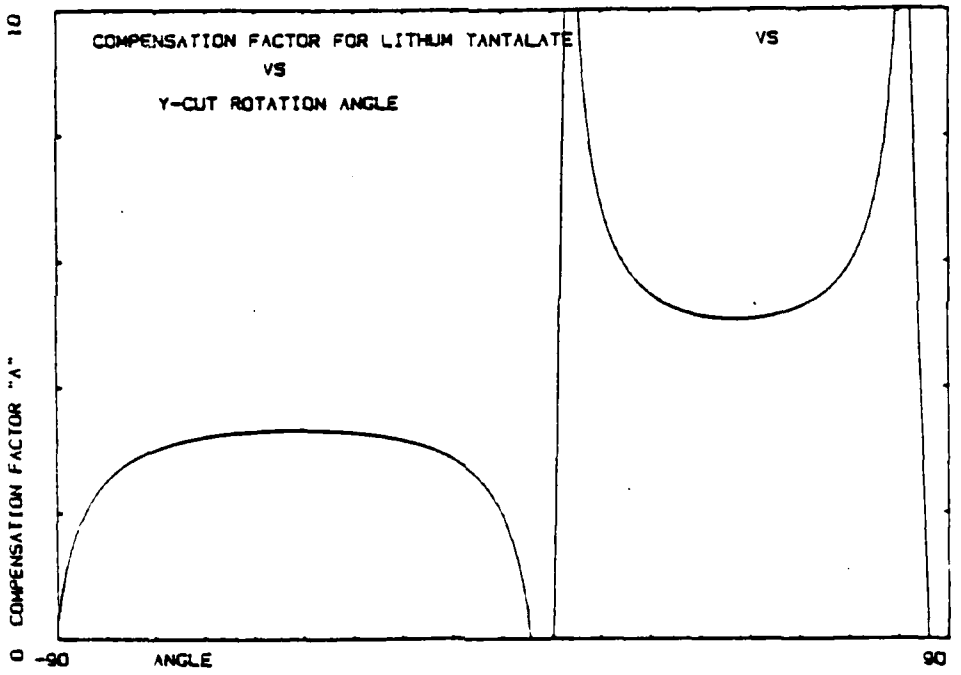

FIGURE 6

As in Fig. 4, for lithium tantalate (-90° to 5°, 12° to 83°).

controlled by adjusting the orientation of the quartz substrate—a process which does not allow for slight modifications of the temperature behavior once the crystal substrates are delivered. If STW filters were used they would allow greater freedom in selecting the crystal orientation, and the temperature behavior could be adjusted by selecting the grating dimensions. This would allow the selection of the ET-cut (maximum coupling) while still giving the required temperature behavior.

(d) Temperature-Frequency Characteristics of Grooved Grating STW Resonators

Fractional frequency change ($\Delta F/F$) versus temperature curves for a resonator, are calculated from the resonator resonant frequency condition, and are referenced to the turnover frequency F_0. The turnover frequency is the frequency at which the temperature derivative of frequency goes to zero. The resonant frequency condition is

$$F_{(T)} = NV_{stw}/2L_r \tag{16}$$

where V_{stw} is the STW velocity, L_r is the length of the resonator region in Fig. 2, and N is an integer. From the temperature coefficients available for quartz in the literature[10] the temperature dependence of the V_{stw} and L_r are calculated and used to evaluate

$$\Delta F/F = \frac{F_{(T)} - F_0}{F_0} \tag{17}$$

for various grating compensation geometries determined by Eq. 14.

Figure 7a shows the effect of grating compensation at a Y-cut rotation angle near the AT-cut (SSBW temperature compensated at 25°C). The turnover temperature for SSBW on a 37 rotated Y-cut quartz crystal is at 85°C. By adding a grating to create a STW we effectively shift the turnover temperature to a lower temperature. Proper selection of the grating height shifts the turnover temperature to room temperature (25°C) and thus temperature compensates STW propagation normal to the X-axis on 37 rotated Y-cut quartz.

Figure 7b is a comparison of STW temperature compensation at several different rotated Y-cut orientations. The ET-cut[13] (maximum piezoelectric coupling) has a $\Delta F/F$

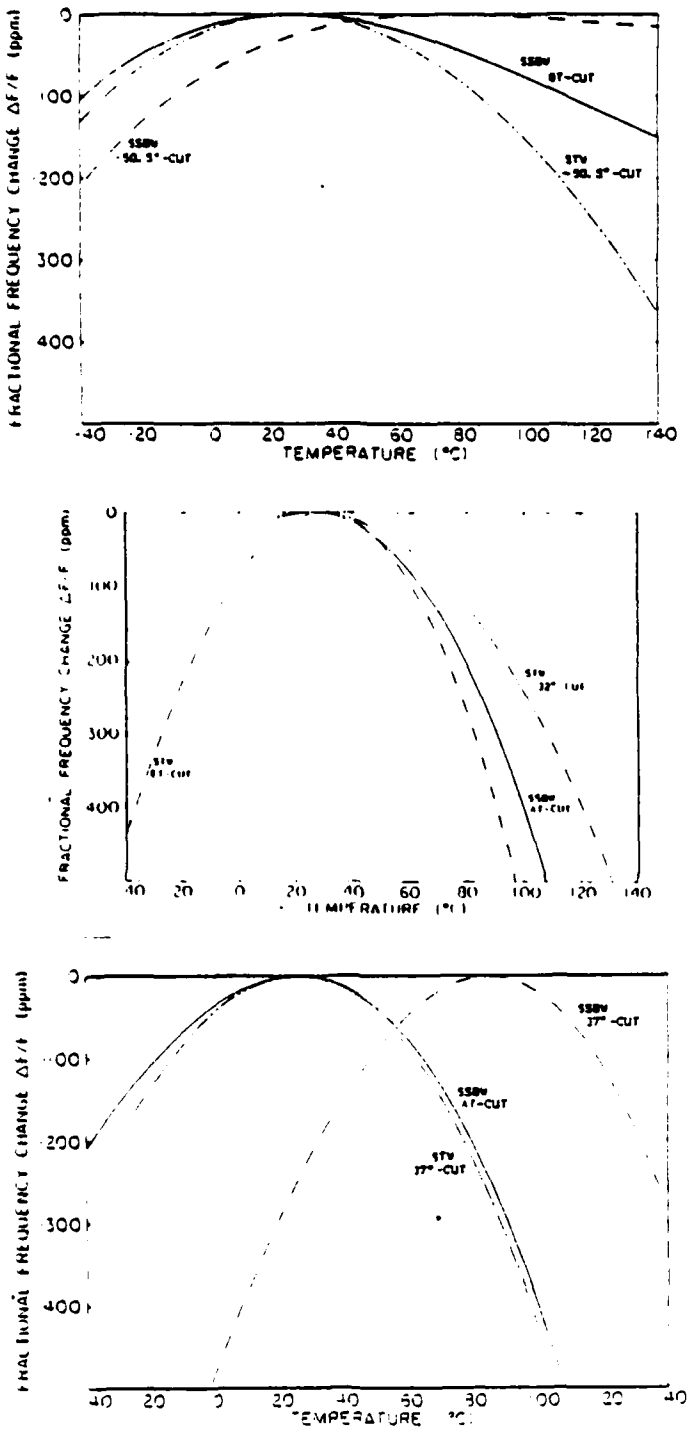

FIGURE 7

Examples of $\Delta F/F$ curves for STW in quartz. (a) Turnover temperature shift due to the STW grating near the AT-cut; (b) Comparison of the STW temperature compensation for the ET-cut and the 32° cut with the SSBW AT-cut; (c) The effect of the STW grating on the cubic behavior of the -50.5° cut.

curve that is not as flat as the SSBW AT-cut, while the 32° cut (large surface wave velocity) has a $\Delta F/F$ curve that is flatter than the AT-cut and thus has a better temperature characteristic near the turnover temperature.

Figure 7c shows the cubic behavior of the -50.5° rotated Y-cut SSBW. This cubic behavior is lost when the grating is introduced to temperature compensate the wave. Because of this the $\Delta F/F$ curve is not as flat as the SSBW BT-cut. (However, it should be noted that the temperature curve is flatter for STW on this orientation than for any of the cases considered in parts (a) and (b) of the figure.) This loss of the cubic behavior is also observed when the SSBW is compensated using metal overlays.[14]

(e) Surface Transverse Wave Theory for Mass Loading Gratings

Surface transverse wave propagation under a mass loading grating differs from the grooved grating in several ways. In the absence of the grating the solution is a SSBW, as it was for the grooved grating, but the slowing effect of the mass loading is two-fold. The first slowing effect is that of the grating and has characteristics similar to the grooved grating STW described above. In addition, a second slowing effect is due to the different shear wave velocities in the substrate and the strip. If the velocity in the strip medium is slower than that of the substrate, the surface wave propagating beneath the strip has an additional slowing term which is dependent on the stiffness difference and the density difference between the two materials. This additional slowing effect is similar to the slowing of Love wave propagation along the surface of a quartz substrate with a thin metal overlay. Both of these slowing effects aid in the trapping of the SSBW to form a mass loading STW. This ability to independently choose the grating material is important because it gives another degree of freedom in designing for temperature compensation.

The derivation of the mass loading STW velocity differs from the grooved gratings in the application of the Datta-Hunsinger boundary condition used to find the space harmonic equation. For mass loading the stress T'_{xz} and density ρ' in the strip in Eq. 4 differ from those of the substrate, and thus the coupling terms K_{nq} are more complicated. Making the same resonance approximation as in the derivation for grooved STW derivation, where only the 0th and -1th space harmonics were considered non-negligible, the following coupled

equations are obtained.

$$\begin{aligned}\left[c_{eff}\beta_{-1}-\rho\omega^2\right]^{1/2}a_{-1} &= K_{-1-1}a_{-1}+K_{0-1}a_0\\ \left[c_{eff}\beta_0-\rho\omega^2\right]^{1/2}a_0 &= K_{-10}a_{-1}+K_{00}a_0\end{aligned} \tag{18}$$

where

$$K_{-10}=-K^*_{0-1}=\omega h\rho'\frac{\Lambda}{\pi}\left[1-\left(\frac{V_m}{V_s}\right)^2+\frac{2\pi}{\Lambda\beta_0}\left(\frac{V_m}{V_s}\right)^2\right]$$

$$K_{00}=K_{-1-1}=j\omega h\rho'\frac{\Lambda}{2}\left[1-\left(\frac{V_m}{V_s}\right)^2\right]$$

$V_m =$ the wave velocity in the mass loading strip.

To calculate the STW dispersion curves from Eq. 18, a small frequency perturbation $\delta\omega$ and a small propagation constant perturbation $\delta\omega$ are assumed relative to the 0th and -1th space harmonic resonant point (R in Fig. 3). This leads to the following mass loading coupled wave dispersion relation

$$\left[\left(\frac{\delta\omega}{V_s}\right)^2-\delta\beta^2\right]^{1/2}=\frac{K_{-10}K_{0-1}-K_{00}^2}{\left(\frac{2\rho c_{66}\Lambda^3}{\pi}\right)}+\frac{K_{00}}{\sqrt{\frac{2\rho c_{66}\Lambda^3}{\pi}}}\left[\left(\frac{\delta\omega}{V_s}+\delta\beta\right)^{1/2}+\left(\frac{\delta\omega}{V_s}-\delta\beta\right)^{1/2}\right] \tag{19}$$

Using this dispersion relation, and making the near stop band approximation, an analytical relation for the mass loading STW velocity can be found. This is

$$V_{stw}=\frac{V_s\omega}{\omega_0-\left[(\omega_0-\omega)^2-(V_sM)^2\right]^{1/2}} \tag{20}$$

where

$$M=\frac{2\pi}{\Lambda}\left(\frac{h}{\Lambda}\right)^2\frac{\rho V_s^2}{c_{66}}\left(\frac{\rho'}{\rho}\right)^2\left[\left(\frac{1+(V_m/V_s)^2}{2}\right)^2-\left(\frac{\pi}{4}\left(1-\left(\frac{V_m}{V_s}\right)^2\right)\right)^2\pm\frac{\pi}{4}\left(1-\left(\frac{V_m}{V_s}\right)^4\right)\right]$$

Note this has the same form as for the grooved STW, but with a modified coupling constant. Again, as in the grooved grating case, the following condition must be satisfied for STW propagation in the pass-band

$$(\omega_0-\omega)^2>(V_sM)^2 \tag{21}$$

The STW velocity for the mass loading grating reduces to the velocity for the grooved grating when the density and stiffness of the strip are the same as the substrate, as expected.

With the grooved STW, this result can be applied to an investigation of the temperature characteristics of mass loading STW propagation normal to the X-axis on rotated Y-cut trigonal crystal plates. However such an investigation is, in itself, not beneficial at this time because the mass loading theory described above is incomplete from a temperature analysis point of view. The theory fails to include the possibility of the mass loading material having thermal expansion coefficients that differ from the substrate material. Preliminary stress strain calculations indicate that the effect of these different thermal expansion rates will have a greater effect on the temperature behavior than that of the grating geometry and material slowing effects in the mass loading grating STW theory given above. This thermal expansion effect, along with methods to incorporate it into the mass loading, STW theory are described in the following section.

III. STATIC STRAIN EFFECTS ON MASS LOADING GRATING STW PROPAGATION

(a) General Considerations

In a metal strip or mass loading grating the grating is made of a different material than the substrate and thus will, in general, have different acoustic and thermal characteristics. A difference in thermal expansion coefficients causes the metal strip to expand or contract at a different rate than that of the substrate. If the metal strip continues to adhere to the substrate without cracking, the substrate and the metal strip must undergo small deformations to allow for the different thermal expansion rates. Because this deformation or strain field varies slowly with time compared to the strain fields of the propagating STW, it is referred to as a static strain. This static strain is a function of the temperature, the thermal and elastic characteristics of the two dissimilar materials, and the method used to deposit the metal strips on to the substrate. If the deformation or static strain is small (that is if it remains in the linear region of the stress vs. strain curve of the material, Fig. 8), it will have little effect on the STW behavior, other than the change in grating dimensions already accounted for, and thus be negligible. However, if the material

is strained to the point where the stress strain curve is no longer linear then the stress strain relation

$$T_I = c_{IJ} S_J \tag{22}$$

which governs the STW is changed and the STW analysis must be modified to account for this effect. In the case of aluminum strips on quartz, lithium niobate or lithium tantalate this added strain effect is not negligible and must be incorporated into our STW temperature theory to predict accurate STW temperature behavior. This will be done by introducing a temperature-dependent static strain term in the crystal stiffness constants used in evaluating the STW velocity. A discussion on this static strain term follows.

(b) Static Strain Theory on Overlay Gratings

The static strain theory developed here is based on the assumption that the particle displacement is the superposition of a small dynamic displacement and a larger static displacement. The small dynamic displacement is due to the stress fields of the acoustic wave and the large static displacement is caused by the forces created by differential expansion of the metal strips and the crystal substrate. This theory can be thought of as the mechanical analog to the small signal circuit analysis of electronic circuit theory where there is a small AC single superimposed on a large DC bias. In each case a linear theory is used to describe the small signal behavior even though the large signal behavior is nonlinear.

This static strain theory begins with the assumption that the total particle displacement field near the interface of the two materials is a superposition of two particle displacement fields. The first is a static displacement caused by crystal particle displacements relative to the natural or initial crystal particle positions. This static displacement includes any crystal deformation experienced during processing of the device, caused by previous thermal expansion history. The second is the dynamic particle displacement which is caused by the stress fields of the STW. The static strain is assumed to vary with time at a very slow rate compared to the strain fields of the STW and is assumed to be constant with time relative to the dynamic displacement. The spatial and temporal particle displacement

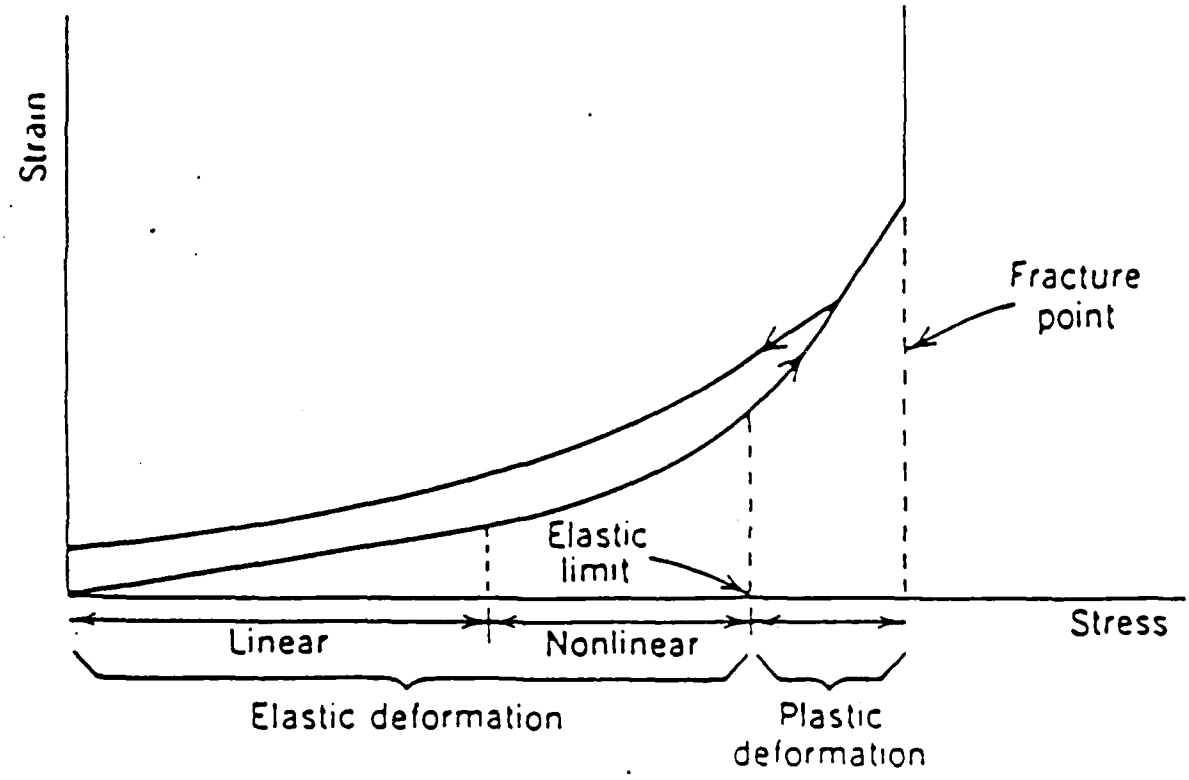

FIGURE 8

Typical stress-strain relation for a solid material.

can then be written

$$U_{(x,y,z,t)} = U^s_{(x,y,z)} + U^d_{(x,y,z,t)} \tag{23}$$

where U^s is the static stress, which is independent of time, and U^d is the dynamic displacement which is a function of time. To justify the small signal analysis, the magnitude of the dynamic displacement must be much smaller than that of the static strain.

$$U^s \gg U^d \tag{24}$$

In addition it is assumed that the net displacement is still governed by the linear acoustic field equations

$$\begin{aligned} \nabla \cdot T &= \rho \frac{\partial^2 U}{\partial t^2} \\ \nabla_s U &= S \end{aligned} \tag{25}$$

The constitutive stress strain relation includes the nonlinear stress strain behavior and has the form

$$T_I = c_{IJ} S_J + c_{IJK} S_K S_J \tag{26}$$

where c_{IJ} and c_{IJK} are the second- and third-order elastic constants which can be found in the literature.[10,11,15,16,17] Substituting the assumed particle displacement U into the strain relation Eq. 25 we find

$$S = S^s + S^d = \nabla_s U^s + \nabla_s U^d \tag{27}$$

which has the same form as the particle displacement (i.e., a superposition of a large static strain and a small dynamic strain). If we substitute this strain into the constitutive relation we find the stress to be of the form

$$T_I = T^s_I + T^d_I \tag{28}$$

where

$$\begin{aligned} T^s_I &= c_{IJ} S^s_J + c_{IJK} S^s_J S^s_K \\ T^d_I &= c_{IJ} S^d_J + c_{IJK} S^d_K S^d_J + c_{IJK} S^s_K S^d_J \end{aligned}$$

If it is assumed that the second-order term in the dynamic stress equation is negligible, then the dynamic constitutive relation becomes

$$T_I^d = c_{IJ} S_J^d + c_{IJK} S_K^s S_J^d \tag{29a}$$

$$T_I^d = [c_{IJ} + c_{IJK} S_K] S_J^d \tag{29b}$$

Substitution of these constitutive relations into the divergence of stress relation (Eq. 25a) separates the analysis into two problems, a static problem

$$\begin{aligned} \nabla T^s &= 0 \\ T^s &= c_{IJ} S_J^s + c_{IJK} S_K^s S_J^s \end{aligned} \tag{30}$$

and a dynamic problem

$$\begin{aligned} \nabla \cdot T^d &= \rho \frac{\partial^2 U^d}{\partial t^2} \\ T^d &= c_{IJ}^{eff} S_J^d \end{aligned} \tag{31}$$

where

$$c_{IJ}^{eff} = c_{IJ} + c_{IJK} S_K^s$$

The dynamic acoustic equation can be applied to the STW problem, resulting in a wave equation that includes the static stress effect

$$\nabla \cdot c^{eff} : \nabla_s U^d = \rho \frac{\partial^2 U^d}{\partial t^2} \tag{32}$$

This is a simplified static strain analysis resulting in a wave equation of the form used in the STW theory described. This allows the addition of the static strain effect to be readily incorporated into the STW temperature theory already prescribed. A more detailed discussion of the static strain effects, including changes in the material density and nonlinear acoustic field equations, can be found in reference 18.

(c) Nonuniformity of Static Strain in the Substrate

If the effective stiffness has a constant uniform value throughout the crystal substrate, then the problem in Eq. 32 has the same solution as the previous STW solution, but with modified stiffness values. However the static strain field imposed by static forces on the

crystal surface is not uniform throughout the crystal substrate and such an assumption needs justification.

These static strains are expected to decay exponentially into the bulk of the crystal, to vary periodically about an average value along the direction of STW propagation, and to be uniform in the direction of the metal strip fingers. The stiffness along the STW propagation direction would be expected to increase when the crystal strain is in compression (i.e., underneath a grating tooth) and then decrease when the crystal strain is in expansion (between the grating teeth) or vice versa, depending on the expansion rates of the two materials. Over a region of many grating periods this periodic increase and decrease of the stiffness value would average out to be the unperturbed stiffness value which is uniform along the direction of the wave propagation. In other words the effect of strain along the STW propagation direction tends to cancel. This leaves the strain normal to the STW propagation direction—that is, parallel to the strips. In a practical STW device the grating width is much wider than the STW wavelength, and in the theoretical STW device the width is infinite. In this case the static strain and thus the effective stiffness values should not change appreciably within a few wavelengths of the surface. If the grating height is sufficient to trap the STW energy within a few wavelengths of the surface, the effective stiffness values as seen by the STW are very nearly uniform in the direction perpendicular to the crystal surface. If we limit our discussion to wide aperture devices with many grating fingers and well-trapped STW, we can assume the effective stiffness is uniform in the region of influence of the STW.

(d) Estimates of the Effect of Static Strain on STW Temperature Characteristics

The major strain component caused by the expansion or contraction of the metal strip fingers will be parallel to the fingers and transverse to the STW propagation direction. This strain component, acting over the full aperture, has large particle displacements and gives the major contribution to the nonlinear stress strain relation affecting the change in the stiffness values. Those strain components perpendicular to the fingers tend to be relieved by the gaps between the metal fingers, and do not have the opportunity to build

up the large particle displacements of the components parallel to the fingers. Thus they will have a smaller effect on the STW velocity. To maintain simplicity in the analysis, the smaller strain component oriented along the wave propagation direction (or perpendicular to the fingers) is neglected, and the static strain caused by the metal strips is assumed to be uniform and acting parallel to the fingers (or in the X-direction, so that the static strain is S_1).

The effective trigonal crystal stiffness constants, used in the STW calculations of section I, for a uniform S_1 strain, become

$$\begin{aligned} c_{55}^{eff} &= c_{55} + c_{551} S_1 \\ c_{56}^{eff} &= c_{56} + c_{561} S_1 \\ c_{66}^{eff} &= c_{66} + c_{661} S_1 \end{aligned} \tag{33}$$

From the crystal symmetry

$$\begin{aligned} c_{551} &= c_{155} \\ c_{561} &= [-2c_{111} - c_{112} + 3c_{222}]/4 \\ c_{661} &= [c_{114} + 3c_{124}]/2 \end{aligned} \tag{34}$$

and c_{IJK} can be found in the literature for quartz[15] and lithium niobate.[17]

Stress changes as high as 150 million newtons per square meter per degree celsius have been observed in thin films of aluminum.[19] A stress change of this magnitude would result in S_1 strain changes on the order of 1700 ppm in quartz and 750 ppm in lithium niobate. Substituting a S_1 strain of just 100 ppm into Eq. 33 gives rise to a change in the quartz elastic constant c_{55} of 300 ppm per degree C and the lithium niobate elastic constant c_{55} of 100 ppm per degree C. Comparison with the elastic temperature coefficients of 177 ppm per degree C for c_{55} in quartz[11] and 430 ppm per degree C for c_{55} in lithium niobate[10] shows that static strain effects are far from negligible. Thus, to accurately predict the acoustic wave temperature behavior of mass loading gratings, this static strain effect must be included in any temperature analysis.

Anomalous temperature behavior in acoustic devices has long been observed at Hewlett-Packard.[20] Theoretical temperature coefficients and the measured parameters were

found to be in disagreement, and temperature-dependent static strain was proposed as the cause of this discrepancy. An example of this unexpected behavior was observed in quartz SAW resonators. Identical resonators exhibited varying drifts in resonant frequency with age. It was discovered that if the resonators are put though an annealing process before the final frequency trimming step, this frequency drift can be reduced. This observed behavior can be explained by static strains. The drift in frequency is caused by a relaxation with aging of the very large initial stresses in the aluminum strips. During the annealing processes the initial stress is reduced so that the change in strain with aging is greatly reduced. After annealing, all the devices are brought to the same static stress level, so that the behavior observed in each individual device is consistent with the other identical devices. These phenomena indicate the importance of considering static stress in this temperature compensation investigation.

Before the effective stiffness result described above can be substituted into the earlier STW theory to incorporate the effect of the static strain S_1 on the wave velocity, it is necessary to determine the strain S_1 and its temperature variation. One method is to consider the published thermal expansion rates and elastic constants of the substrate and the aluminum, and then to calculate the induced strain, assuming no strain at an initial temperature. This approach is not adequate for several reasons. First, the thermal expansion and elastic coefficients of thin aluminum strips are not the same as the published values for bulk aluminum. Also, in thin films these coefficients vary greatly with film thickness and composition. In addition, the initial strain state of the device is a nonzero because of the processing steps and past temperature history. This initial strain state may vary greatly from device to device and has to be determined to characterize the temperature behavior of each new device.

For these reasons S_1 must be determined empirically for a given device. Once the strain state of the device has been determined the effective stiffness can be substituted into the STW theory described previously and a prediction made of the STW temperature behavior. Once the experimentally-determined metal strip grating STW temperature characteristics are obtained they can then be applied to the STW temperature compensa-

tion theory described above. The difficulty is that the static strain versus temperature properties depends on the grating geometry as well as on the material properties.

Fabrication of experimental STW devices for this program was started at Hewlett-Packard during the summer of 1985. Both grooved STW gratings and metal strip grating devices were projected. However, due to Hewlett-Packard's work scheduling requirements at that time, none of the devices were completed. The etching process for the grooved grating was never begun and the metal strip devices fabricated were not wire-bonded and packaged. At present there exist 14 unfinished metal strip grating devices. These consist of aluminum strip gratings with a period of 4 microns on ST-cut quartz substrate, with interdigital transducers oriented to launch STW normal to the X-axis. The center stop band frequency of the grating devices is near 670 MHz. There are five different metal thickness 3000, 2000, 1400, 1000, and 730Å. They still need to be wire-bonded and packaged before temperature measurements can begin. Further work on the STW static strain theory will be published at a later date as a Ph.D dissertation and, if possible, measurements will be made. A copy of this work will be submitted to the Paul Carr at RADC as a follow-up to this report.

IV. NORMAL MODE SURFACE ACOUSTIC GRATING WAVES (SAGW)

(a) Overview of Grating Wave Characteristics

In rotated Y-cut trigonal crystals, surface skimming bulk waves (SSBW) exist only for propagation normal to the X-axis. Addition of a surface grating converts these surface skimming bulk shear waves into pure shear (or transverse) surface waves (STW). As noted earlier, temperature-compensation of these waves on quartz, lithium niobate, and lithium tantalate can be achieved by proper selection of the crystal orientation and the grating dimensions. For lithium niobate and lithium tantalate, however, these cuts are not piezoelectrically active, and cannot be excited with an interdigital transducer.

Piezoelectric coupling is present for propagation along the X-axis of rotated Y-cut lithium niobate and lithium tantalate crystal plates,[21,22] and these cuts are found to have

the attractive feature of very strong piezoelectric coupling ($\Delta V/V = 0.02776$ for -48° rotated Y-cut[25]). For this direction of propagation pure SSBW and STW exist only for certain specific rotation angles[22,23] and for most angles only leaky waves exist. Consequently, to study temperature compensation of surface grating waves on piezoelectrically active cuts it is necessary to extend the previous theory (developed for pure shear waves, polarized parallel to the crystal surface) to the case of general polarizations. Two approaches will be followed.

The first referred to as *normal mode surface acoustic grating wave theory* consists of a perturbation theory which allows for an arbitrarily polarized Rayleigh surface wave as the unperturbed wave solution. When a surface grating is present it perturbs the Rayleigh wave propagation, resulting in a surface acoustic grating wave (SAGW). This normal mode theory is discussed in more detail below.

The second is referred to as *leaky surface wave theory*, and consists of a direct numerical solution to the differential wave equation, and boundary conditions for arbitrarily polarized surface wave propagation under grooved gratings on anisotropic crystals. In general some of these orientations cannot support true surface waves on a smooth surface because the wave radiates or leaks power in to the bulk of the substrate. This leaky wave theory will be discussed in a later section.

(b) Normal Mode SAGW Theory

This approach assumes surface acoustic grating wave propagation on a thick anisotropic crystal plate. The assumption of a plate of finite, but large, thickness is needed to obtain a complete basis set of normal modes. On a thick plate the Rayleigh mode is the same as a Rayleigh wave on a semi-infinite substrate, but it is a member of the family of orthogonal modes of the plate. This normal mode property of the Rayleigh wave greatly facilitates the analysis of Rayleigh grating wave propagation. Following the Floquet method used for the STW case[24] one can represent the particle displacement velocity $V_{(x,z)}$ and stress $T_{(x,z)}$ fields by the space harmonic expansion

$$\begin{bmatrix} v_{(x,z)} \\ T_{(x,z)} \end{bmatrix} = \sum_n a_n \begin{bmatrix} v_n(z) \\ T_n(z) \end{bmatrix} \exp(-i\beta_n x) \tag{35}$$

where

$$\beta_n = \beta_0 + \frac{n2\pi}{d}$$

Without loss of generality, each individual space harmonic may be expanded in terms of a series of plate mode functions or "normal mode functions" (including Rayleigh and B-G waves). This gives

$$a_n \begin{bmatrix} v_n(z) \\ T_n(z) \end{bmatrix} e^{-i\beta_n x} = \sum_\nu \begin{bmatrix} v_{n\nu}(z) \\ T_{n\nu}(z) \end{bmatrix} e^{-i\beta_n x} \tag{36}$$

where each of the plate mode wave functions ν satisfies the acoustic field equation for a smooth surface at a particular frequency $\omega_{n\nu}$,

$$\begin{bmatrix} 0 & \nabla \\ \nabla & 0 \end{bmatrix} \begin{bmatrix} v_{n\nu}(z) \\ T_{n\nu}(z) \end{bmatrix} e^{-i\beta_n x} = i\omega_{n\nu} \begin{bmatrix} \rho & 0 \\ 0 & s \end{bmatrix} \begin{bmatrix} v_{n\nu}(z) \\ T_{n\nu}(z) \end{bmatrix} e^{-i\beta_n x} \tag{37}$$

To develop coupled space harmonic equations for a grating surface, Eq. 35 and Eq. 36 are substituted into the acoustic field equations. The result is reduced to a set of coupled equations in terms of the plate mode harmonic amplitudes a_n by using the orthogonality relations of the space harmonics and the plate modes, and then integrating throughout the thickness of the substrate and over one period of the grating. The space harmonic equation is further simplified by noting that the boundary conditions at the bottom of the plate are those for a free surface, and the boundary conditions at the top of the plate are given by the Datta-Hunsinger grating theory.[8] Using the above simplifications, the acoustic field equations reduce to a set of linear equations coupling the space harmonic mode amplitudes $a_{m\mu}$, $a_{n\nu}$

$$(\omega - \omega_{m\mu}) a_{m\mu} = \sum_{n\nu} K_{m\mu,n\nu} a_{n\nu} \tag{38}$$

where

$$K_{m\mu,n\nu} = \int_0^\Lambda \frac{i e^{i(\beta_m - \beta_n)z}}{\Lambda U_{m\mu,n\nu}} \left[v^*_{x_{m\mu}} T_{xy_{n\nu}} + v^*_{y_{m\mu}} T_{yy_{n\nu}} + v^*_{z_{m\mu}} T_{zy_{n\nu}} \right]_{y=0} dz$$

$$U_{m\mu,n\nu} = \int_{-b}^0 \left[\rho v^*_{m,\mu} \cdot v_{m\mu} + T_{m\mu} : S^E : T_{m\mu} \right] dy \qquad \omega_{m,\mu} = V_\mu \beta_m$$

These are known as the space harmonic equations.

As in the STW case an approximate theory for shallow gratings is obtained by considering only the space harmonic interaction near the first resonance point. With this near-resonance assumption, the infinite set of space harmonic equations can be reduced to two equations for a pair of coupled harmonics, the 0th space harmonic and the -1th space harmonic. The coupled normal mode space harmonic equations for the Rayleigh grating wave are then (Appendix A1)

$$\begin{aligned}(\omega - V_r\beta_{0,R})a_{0,R} &= a_{-1,R}K_{0,-1} + a_{0,R}K_{0,0} \\ (\omega + V_r\beta_{-1,R})a_{-1,R} &= a_{-1.R}K_{-1,-1} + a_{0,R}K_{-1.0}\end{aligned} \tag{39}$$

where

$$K_{0,0} = K_{-1,-1} = -\frac{\rho\pi^2 V_R^3}{8\Lambda}\left(\frac{h}{\Lambda}\right)\frac{|U_y|^2}{P_r}$$

$$K_{-1,0} = -K_{0,-1}^{*} = \frac{i\rho\pi}{4\Lambda}V_R^3\left(\frac{h}{\Lambda}\right)\left[\frac{(U_y^{*})^2}{P_r} + 2\frac{(U_z^{*})^2}{P_r}\right]$$

and

a_o and a_{-1} are the space harmonic amplitudes;

$\beta_{0,R}$ and $\beta_{-1,R}$ are the space harmonic wave numbers;

V_R = the normal mode velocity (Rayleigh velocity);

ω = the grating wave frequency;

$U_y/P_r^{1/2}$ = normalized Y-polarized displacement;

$U_z/P_r^{1/2}$ = normalized Z-polarized displacement;

ρ = the density of the crystal;

h = the height of the surface grating;

Λ = the period of the surface grating.

To investigate the temperature characteristics of grating Rayleigh waves an analytical expression for the grating wave phase velocity must be obtained from Eq. 39. To simplify the solution of Eq. 39 it is assumed that the wave number of the grating wave does not deviate much from the normal mode (Rayleigh) wave number. This simplification permits expression of the coupling constants K_{0-1} and K_{-10} as true constants, independent of the

wave number. This is analogous to the simplification made in the STW theory, where the term neglected was of second order and a deviation of 10% in the wave number caused a deviation in the coupling constant of only 1%. It was also assumed the displacement velocity under a grating tooth was equal to the velocity between the grating teeth. This assumption was made by Datta-Hunsinger in calculating the boundary conditions under the grating; and it must also be made here, to use their boundary conditions. After making these assumptions, the surface acoustic grating wave phase velocity was found to be (Appendix A2)

$$V_{\mathrm{SAGW}} = V_R - \frac{h}{\Lambda}\frac{\rho V_R^3}{4}\left[\frac{\pi}{2}\frac{|U_y|^2}{P_r} - \left|\frac{U_y^2}{P_r} + \frac{2U_z^2}{P_r}\right|\right] \tag{40}$$

The quantities V_R, $U_z/P_r^{1/2}$,and $U_y/P_r^{1/2}$ in Eq. 40 can be obtained from existing computer programs, such as the one used by Slobodnik[25] or Andle.[26] From numerical data at several different temperatures, the temperature coefficients of V_R, U_z/P_r, and U_y/P_r can be estimated. Using these temperature coefficients, along with those for the crystal expansion coefficients found in the literature,[27,28] an analytical expression for the temperature dependence of the surface acoustic wave velocity under a shallow grating can be obtained.

(c) Temperature Compensation of SAGW

(i) General Formulation

The Temperature Coefficient of Delay (TCD) equation

$$\mathrm{TCD} = \alpha - \frac{1}{V_{\mathrm{SAGW}}}\frac{dV_{\mathrm{SAGW}}}{dT} \tag{41}$$

is used to calculate the grating dimensions that give a zero temperature coefficient of delay. Knowing the temperature dependence of the SAGW phase velocity discussed above, and the expansion coefficient in the direction of wave propagation, one can solve the above TCD equation for the grating height-to-period ratio that gives a zero temperature coefficient of delay. This compensating height-to-period ratio was found to be (Appendix A3)

$$\frac{h}{\Lambda} = \frac{V_{R_{TC}} - \Lambda_{TC}}{\frac{\rho\pi V_R^2}{8}\frac{|U_y|^2}{P_r}(A_{TC}) + \frac{\rho V_R^2}{4}\left|\frac{U_y^2}{P_r} + \frac{2U_z^2}{P_r}\right|(B_{TC})} \tag{42}$$

where

$$A_{TC} = \rho_{TC} + h_{TC} + 3V_{R_{TC}} + 2\left(\frac{|U_y|}{P_r^{1/2}}\right)_{TC} - 2\Lambda_{TC}$$

$$B_{TC} = \rho_{TC} + h_{TC} + 3V_{R_{TC}} + \left|\frac{U_y^2}{P_r} + \frac{2U_z^2}{P_r}\right|_{TC} - 2\Lambda_{TC}$$

(ii) SAGW on Lithium Niobate

The SAW data for lithium niobate provided by Rick Webster at RADC, was used to plot the height-to-period ratio needed to temperature compensate a SAGW propagation normal to the X-axis on rotated Y-cut lithium niobate. This quantity is plotted versus rotation angle in Fig. 9. The value of the smallest height-to-period ratio is approximately 4 at an angle of -35° ($\Delta V/V$ 74% of the maximum rotated Y-cut $\Delta V/V$, Reference 25). This shows that, for a grating on lithium niobate to completely temperature-compensate the delay at room temperature, the "grating teeth" must be about eight times higher than they are wide.

This result is a demonstration of a grating structure used to reduce the SAW TCD and, in the case of deep gratings, to achieve complete temperature compensation of SAW devices on the higher coupling materials. However, the grating dimensions needed to achieve this theoretical temperature compensation calculated with the preceding theory must be examined critically. First, the capabilities of today's technology do not allow fabrication of grooved gratings with a height-to-width aspect ratio of eight. Even if these deep gratings could be fabricated, the calculated dimensions of such a grating predicted by the preceding theory must be questioned. The theory uses the Datta-Hunsinger perturbation formula to calculate the stress fields under the grating. This formula assumes a small grating height, and thus would not give accurate results for deep gratings. To achieve accurate predictions of the deep grating heights a more detailed method must be used to calculate the stress fields beneath the grating teeth. In lieu of trying to fabricate these deep gratings, should they be calculated, shallow grating perturbation theory will be used to look for shallow grating structures that can be manufactured using today's technology, with the understanding that deep gratings can possibly aid the temperature compensation, but may

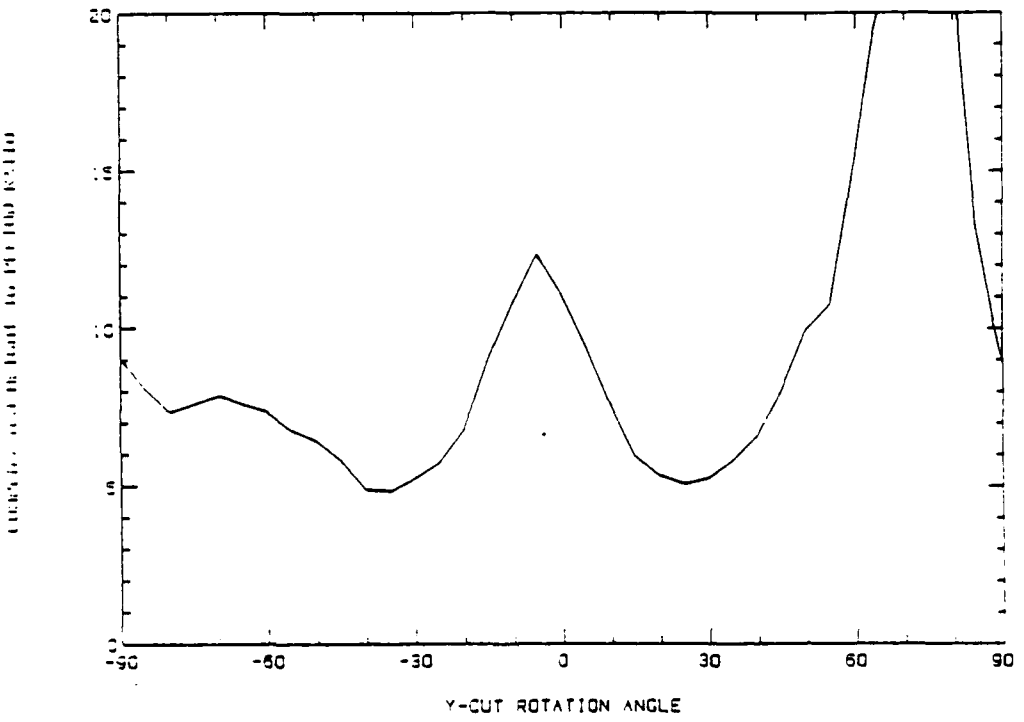

FIGURE 9

Compensation height-to-period ratio needed to achieve a zero TCD for SAGW propagation normal to the X-axis on rotated Y-cut lithium niobate using the Webster data.

not have the exact height value needed to achieve complete temperature compensation. Another objection to the above theory is that it does not consider the piezoelectric effect on the wave propagation. This effect cannot be automatically neglected in the case of the higher coupling materials, and will be considered in a later section of this report.

Calculations for lithium niobate have been compared using two different sets of SAW data, i.e., the Andle data from the University of Maine and data from Rick Webster at RADC. The quantity compared was the height-to-period ratio needed to achieve a zero TCD for SAGW propagation normal to the X-axis on rotated Y-cut lithium niobate. Leaky bulk shear wave modes can exist on rotated Y-cut lithium niobate plates when the rotation angle falls between 5° and 90°. For this reason, the validity of the SAW data is considered somewhat doubtful in this region. Figure 10 shows the Andle data as a solid curve and the Webster data as a dotted curve. As can be seen in the figure, the calculations are in close agreement over the range of Y-cut angles where no leaky waves exist. In the range of leaky waves (rotation angle from 10° to 90°), both the Andle data and the Webster data were considered invalid because of numerical problems encountered in the computer programs used to calculate the SAW data.

The near stop band assumption made in the previous calculations has also been relaxed, so that calculations may be made at frequencies far removed from the stopband. The resulting TCD equation was more complex than the original and had to be solved using numerical techniques. To aid in the interpretation of the results the propagation constant was first normalized by the stop band propagation constant $\beta_s = \pi/\Lambda$, and then this ratio allowed to deviate from unity. Curves similar to those presented above are plotted for values of β/β_s equal to 1.0, 0.9, and 0.8. It can be seen in Fig. 11 that, as β moves away from the stop band, the height-to-period ratio needed to achieve compensation is increased. Thus we can say the temperature compensating effect of the grating is greatest near the stop band. This characteristic of the temperature compensation effect was proposed earlier in the STW work (Fig. 1) and, as expected, also holds true for the normal mode theory

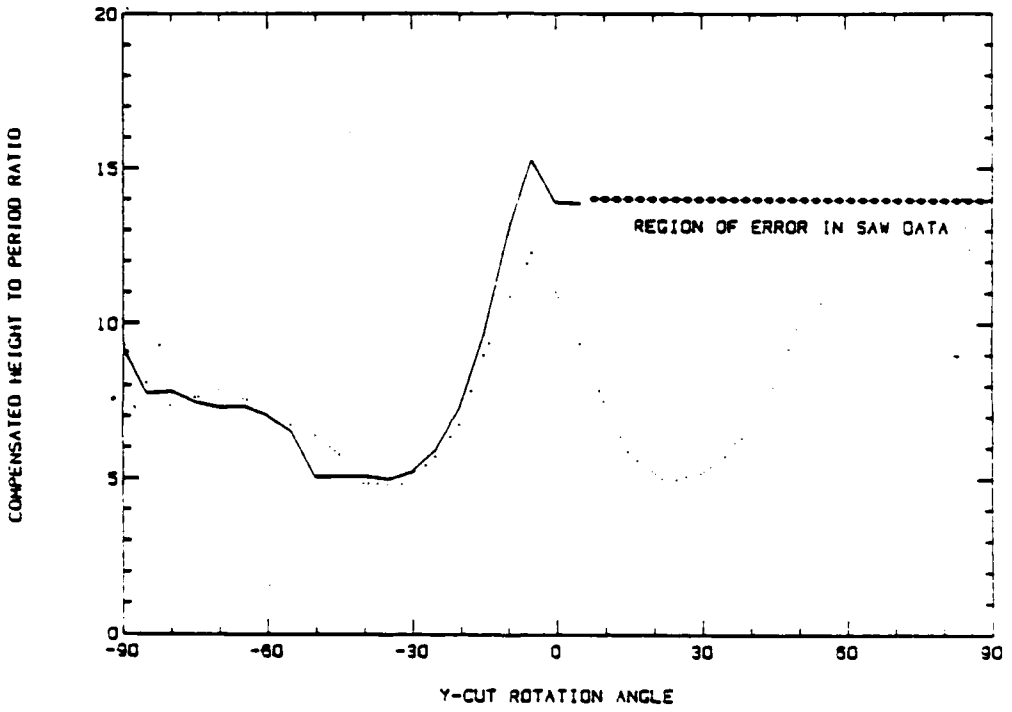

FIGURE 10

Comparison of compensation height-to-period ratio needed to achieve a zero TCD for SAGW propagation normal to the X-axis on rotated y-cut lithium niobate. The Andle data is the solid curve, and the Webster data is the dotted curve.

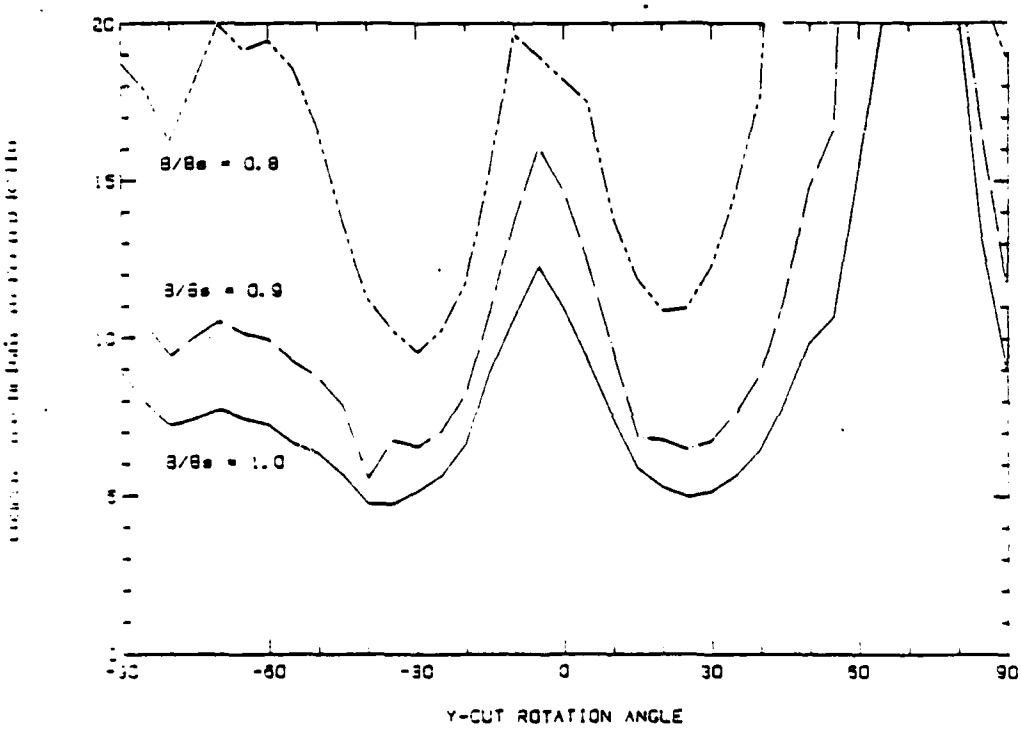

FIGURE 11

Compensation height-to-period ratio needed to achieve a zero TCD for SAGW propagation normal to the X-axis on rotated Y-cut lithium niobate for various values of β/β_s.

(iii) SAGW on Lithium Tantalate

Propagation normal to the X-axis on rotated Y-cut lithium tantalate has also been considered. The Rayleigh surface acoustic wave (SAW) data was obtained from Jeff Andle at the University of Maine. The above theory, together with Andle's SAW data, was used to compute the grating height needed to reduce the temperature coefficient of delay (TCD) to zero at room temperature for varying angles of rotated Y-cut lithium tantalate plates. Height-to-period ratios of the surface grating needed to achieve a zero TCD are shown in Fig. 12 as a function of the Y-cut rotation angle. As expected, the minimum height-to-period ratio required to achieve complete temperature compensation in lithium tantalate (approximately 3 at a Y-cut rotation angle of -80°) is less than that for lithium niobate. However, this result implies a groove depth that is six times the groove width and is subject to the same qualifications as in the case of lithium niobate.

These results confirm that the grating compensation mechanism works in principle for lithium niobate and lithium tantalate. That is to say, the presence of a grating will tend to reduce the magnitude of the TCD. However, the magnitude of the temperature coefficient of lithium niobate at room temperature is so large that the grating height-to-period ratio required to effectively compensate the SAGW are not realizable with present fabrication techniques. In addition, the large height-to-period ratios predicted by this first order perturbation theory are not describable by a first-order theory. For these reasons, an actual prediction of the grating dimensions for temperature compensation requires the incorporation of higher order grating effects into the theory. This would not be practical because of the difficulty in manufacturing these deep gratings, even if they could be accurately calculated.

(d) Piezoelectric Normal Mode Theory for SAGW

To complete the analysis of SAGW it is necessary to include the piezoelectric effect. This theory is based on the Floquet theorem, as was the previous theory. However, instead of expanding in terms of sums of combined plate mode displacement velocity and stress fields as in the previous case

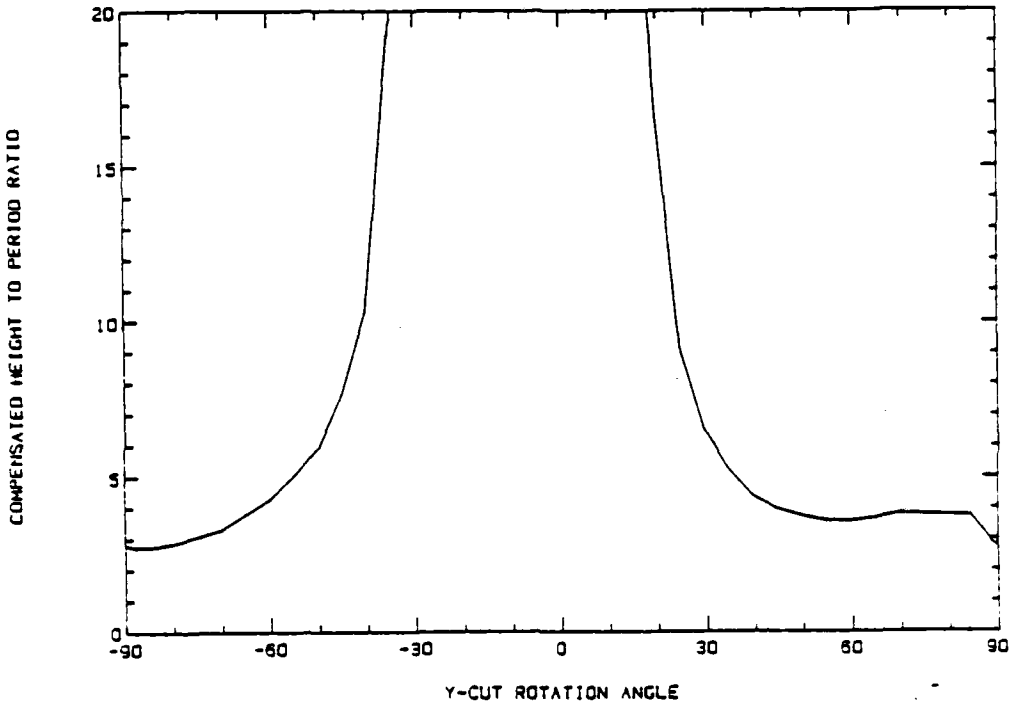

FIGURE 12

Compensation height-to-period ratio needed to achieve a zero TCD for SAGW propagation normal to the X-axis on rotated Y-cut lithium tantalate.

$$\begin{bmatrix} v_{(y,z)} \\ T_{(y,z)} \end{bmatrix} = \sum_{n\nu} a_{n\nu} \begin{bmatrix} v_{n\nu}(y) \\ T_{n\nu}(y) \end{bmatrix} e^{-i\beta_n z} \tag{43}$$

the fields are expanded in individual sums for the displacement velocity, stress, and potential fields.

$$\begin{aligned} v_{(y,z)} &= \sum_{n\nu} a_{n\nu} v_{n\nu}(y) e^{-i\beta_n z} \\ T_{(y,z)} &= \sum_{n\nu} b_{n\nu} T_{n\nu}(y) e^{-i\beta_n z} \\ \phi_{(y,z)} &= \sum_{n\nu} c_{n\nu} \phi_{n\nu}(y) e^{-i\beta_n z} \end{aligned} \tag{44}$$

This expansion method makes for a more elegant solution, where the interpretation of the electrical and mechanical boundary conditions is greatly simplified. The procedure for finding the space harmonic equations is similar to the previous normal mode case, where we substitute Eq. 44 into the quasi-static field equations and make use of the orthogonality of the space harmonics to obtain the space harmonic equations. The resulting space harmonic equation is

$$\int_0^\Lambda \{-v^*_{m\mu} \cdot T \cdot \hat{y} + \phi^*_{m\mu}(i\omega D \cdot \hat{y}) + \phi(i\omega_{m\mu} \cdot \hat{y})^*\} e^{i\beta_m z}\, dz = -i(\omega - \omega_{m\mu})\Lambda U_{m\mu,m\mu} \tag{45}$$

For a nonpiezoelectric problem the electrical terms drop out and we are left with Eq. 38. which we have already solved. For a purely electrical grating $T \cdot n$ is zero, and Eq. 45 becomes

$$\int_0^\Lambda \{\phi^*_{m\mu}(i\omega D \cdot \hat{y}) + \phi(i\omega_{m\mu} D_{m\mu} \cdot \hat{y})^*\} e^{i\beta_m z}\, dz = -i(\omega - \omega_{m\mu})\Lambda U_{m\mu,m\mu} \tag{46}$$

To evaluate the integral on the left side of Eq. 46, we must find the D on the boundary corresponding to each $n\nu$ term in ϕ. As in the mechanical problem, the difficulty is in determining approximate forms of the relation between ϕ and D. Something similar to the Datta-Hunsinger formula, used in the mechanical case, is required. Several approaches to this problem have been considered. One is to use the metal overlay perturbation calculation found in Ref. 29, Eqs. 12.36 and 12.37. These equations, with the electrical surface impedance Z_e, give the potential function and normal D under the strip. This formula is used in the calculation of scattering from a single metal strip,[30] assuming that

the surface boundary conditions are unperturbed at the gap between the strips. Following this approach the left hand side of Eq. 46 becomes

$$\int_0^{\Lambda/2} (\phi^*_{m\mu} i\omega D \cdot \hat{y}) e^{i\beta_m z}\, dz \tag{47}$$

with

$$D \cdot \hat{y} = \sum_{n\nu} a_{n\nu}(-\beta_n(\epsilon_0 + \epsilon_p^T)\phi_{n\nu}) e^{i\beta_n z}$$

Substitution into Eq. 46 gives the space harmonic and mode coupling equations in terms of the grating electrical parameters.

$$(\omega - V_R\beta_m)a_m = -\sum K^E_{mn} a_n$$

$$K^E_{mn} = \begin{cases} \frac{1}{8}\left(\frac{\pi V_R}{\Lambda}\right)^2 \frac{\epsilon_0(\epsilon_0+\epsilon_p^T)}{[\epsilon_0+\epsilon_p^T/\tanh(\beta_r h)]} \frac{|\phi_n|^2}{P_r} & n = m \\ \frac{1}{8}\left(\frac{\pi V_R}{\Lambda}\right)^2 \left[\frac{\epsilon_0(\epsilon_0+\epsilon_p^T)}{\epsilon_0+\epsilon_p^T/\tanh(\beta_r h)}\right] \frac{\phi_n \phi_m^*}{P_r} \left[\frac{1-e^{-i\pi(m-n)}}{i\pi(m-n)}\right] & m \neq n \end{cases} \tag{48}$$

where

$$\epsilon_p^T = \sqrt{\epsilon_x \epsilon_z - \epsilon_{yz}^2}$$

More exact treatments of the electrical grating boundary conditions, including the effects of open and short circuit metal strips, can be found in Ref. 31 and Ref. 32.

As in the mechanical case, it is assumed that all but two space harmonics are negligible near the first stop band. These are the forward-traveling 0th space harmonic and the backward -traveling -1th space harmonic. The analysis is also limited to surface acoustic wave propagation under a grating that has been etched into the surface of the crystal plate (i.e., grooved gratings as opposed to metal strip gratings). The resulting coupled space harmonic equations are then solved to find the change in the SAGW velocity due to the electrical perturbation at the surface, near the first stop band. This gives

$$\Delta V^E_{SAGW} = -V_R \left[\frac{\epsilon_0(\epsilon_0 + \epsilon_p^t)}{\epsilon_0 + \epsilon_p^T/\tanh(\beta_r h)}\right] \frac{|\varphi|^2}{P_r} \left[\frac{1}{8} + \frac{1}{4\pi}\right] \tag{49}$$

If only small surface perturbations are considered, the combined velocity change can be found by adding the changes due to the mechanical and electrical perturbation separately.

Recall the mechanical surface loading calculation neglecting the electrical effects treated earlier (Eq. 40) resulted in the following change in the SAGW velocity due to mechanical loading

$$\Delta V^{M}_{\mathrm{SAGW}} - \left(\frac{h}{\Lambda}\right)\frac{\rho V_R^3}{4}\left[\frac{\pi}{2}\frac{|u_y|^2}{P_r} - |\frac{u_y^2}{P_r} + \frac{2u_z^2}{P_r}|\right] \tag{50}$$

Linearly combining this with the velocity change due to the electrical surface loading in the absence of the mechanical loading (Eq. 48), gives the SAGW velocity due to the combined effect of mechanical loading and electrical loading near the first resonance stop band

$$V_{\mathrm{SAGW}} = V_R + \Delta V^{M}_{\mathrm{SAGW}} + \Delta V^{E}_{\mathrm{SAGW}} \tag{51}$$

Using Eq. 51 in a temperature characteristic analysis analogous to that of the mechanical case, one can solve for the height needed to achieve a zero TCD at room temperature for various rotated Y-cut angles. The result of this calculation is shown as the solid line in Fig. 13. A comparison with the previous SAGW calculation, neglecting piezoelectricity, has also been included as a dotted curve. As can be seen from the curves the addition of a piezoelectricity term had a very small effect on the dimensions needed to achieve complete temperature compensation at room temperature.

(e) Proposed Experimental Device

The above calculations for the grooved grating dimensions required to temperature compensate SAGW propagation normal to the X-axis on rotated Y-cut lithium niobate and lithium tantalate plates, show that a deep grating (at least 3-1 aspect ratio) is required. We suggest that the first experiment demonstrating this method of temperature compensation be made on a -80° rotated Y-cut lithium tantalate plate, with the grooved grating etched as deeply as possible. The temperature characteristics of the device could then be compared to one with a smooth surface. The grating height of the experimental device may not be sufficient to achieve a turnover at room temperature, but it should exhibit a more favorable temperature characteristic. In this way the temperature compensating effect of the grating can be verified. The result of this experiment may then be used to form a judgment of the potential rewards of looking for more sophisticated and effective etching technologies.

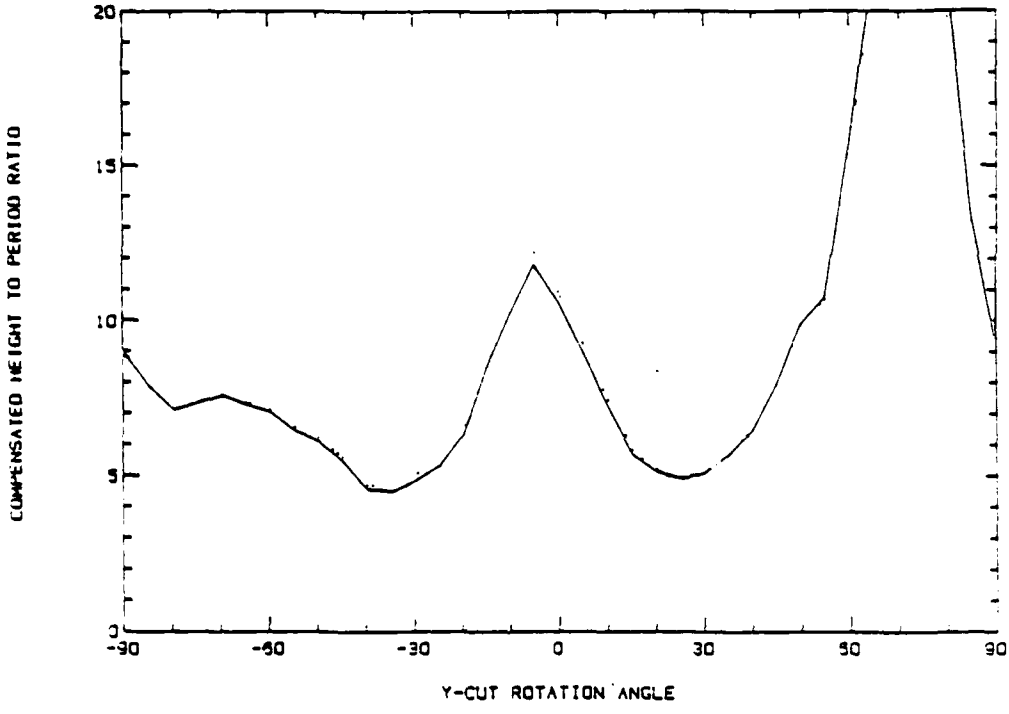

FIGURE 13

Comparison of height-to-period ratio needed to temperature-compensate SAGW propagation normal to the X-axis on rotated Y-cut lithium niobate, with piezoelectricity (solid line) and neglecting piezoelectricity (dotted line).

(f) Metal Strip SAGW

The electrical grating analyses of Ref. 31 has been used in considering the temperature effects of periodic conducting strips on STW and SAGW, with no mass or elastic loading effects. In particular, the results of Ref. 31 for the open circuit case were applied to calculate the surface wave velocity under a conducting grating, where the strip width is equal to the strip separation. This gives

$$V_{\text{SAGW}} = \frac{V_r}{1 + \frac{1}{2}(\Delta V_r / V_r)} \tag{52}$$

where

$$\frac{\Delta V_r}{V_r} = \frac{V_{r\,\text{short}} - V_{r\,\text{open}}}{V_{r\,\text{open}}}$$

This appears as follows in the expression for the TCD.

$$\text{TCD} = \Lambda_{TC} - V_{rTC} + \frac{\Delta V_r / V_r}{2 + (\Delta V_r / V_r)} \left(\frac{\Delta V_r}{V_r} \right)_{TC} \tag{53}$$

The TCD equation consists of an unperturbed surface wave TCD term and a compensating TCD term that is a function of $\Delta V_r / V_r$. Substituting the values of $\Delta V_r / V_r$ for wave propagation perpendicular to the X-axis on 20° rotated Y-cut (70° X-axis cylinder) lithium niobate into the last term of Eq. 53 (see Appendix A4), resulted in a compensating term of -4 ppm/°C. This term will not be able to completely temperature-compensate the unperturbed surface wave term which is greater than 60 ppm/°C. Thus the conducting strip grating could not be used by itself as an effective temperature-compensating method.

In reality the conducting strip could not have an infinitesimal thickness, and the static stress temperature characteristics discussed in Section III will have a predominant effect on the TCD (on the order of 100 ppm/°C). This makes the metal strip electrical shorting effect almost negligible compared to the static stress effect. In order to continue this TCD analysis, the static strain effect would have to be incorporated in to this theory to accurately predict the temperature behavior. This cannot be considered here because of the empirical nature of the static stress theory. However once the static stress temperature behavior has been established this shorting effect could be reconstructed with the effective stiffness values, in the hope of achieving a favorable temperature characteristic.

V. TRAPPING LEAKY SURFACE WAVES

(a) Introduction

The importance of propagation along the X-axis of rotated Y-cut trigonal crystals was noted earlier. Along this direction of propagation there exists a leaky surface wave that reduces to a pure SSBW for certain rotation angles.[33,34,35] These waves have very high coupling constants and have aroused interest because of this fact.[23] Another type of leaky wave reported in the literature is the pseudosurface wave, which reduces to a perfectly trapped Rayleigh wave for certain particular crystal cuts. These exist for a number of materials and crystal cuts (see, for example, References 35 and 36).

Although the existence of the leaky surface waves described in the previous paragraph has been known for some time, especially the pseudo SSBW X-propagating waves on rotated Y-cut lithium niobate and lithium tantalate, they have not been successfully exploited in device applications because of their excessive radiation losses. On quartz, where pure SSBW have found some applications in delay lines at microwave frequencies despite their diffraction losses, a severe limitation is the weak coupling. It has already been noted that pure rotated Y-cut SSBW propagation normal to the X −axis cannot be excited piezoelectrically in high coupling lithium niobate and lithium tantalate crystals. Exploration of the strongly coupled pseudo SSBW on lithium niobate and lithium tantalate is very important to the Air Force's need for low insertion loss broad band delay line devices at microwave frequencies. This requires trapping of the leaky wave on the surface by means of a grating structure. In addition, the same grating might also be used to temperature compensate the quasi-STW realized in this way, as was demonstrated theoretically earlier in this report for SAGW propagation *normal* to the X-axis on rotated Y-cut lithium niobate. An analytical technique developed for this purpose could also extend the range of materials and cuts available for practical applications, by similarly trapping and compensating pseudosurface waves of SAW type on arbitrary crystals.[35,36]

The normal mode SAGW theory presented earlier showed that the theoretical temperature compensation of SAGW propagation normal to the X-axis on rotated Y-cut

lithium niobate is possible with a deep grating. This is an important demonstration of principle, which may well lead to significant practical consequences. However, the normal mode approach cannot be applied to the leaky wave problem discussed above. The reason is that leaky waves exist only on a half-space geometry, where no normal mode structure exists, and thus the normal mode theory cannot be applied.

In view of the ultimate importance of the leaky wave problem, for reasons already stated in the preceding paragraphs, an efficient leaky wave Floquet theory and numerical algorithm has been developed. For a certain height of grating structure the leaky wave becomes a "skimming wave," with no energy leakage. Beyond this height, the wave becomes trapped as a quasi-STW. As a first step in following this leaky wave theory, the height of the grating required to create a skimming wave is found. Before developing this approach, some attention was given to the idea of first calculating the leaky wave fields for a smooth surface (using, for example, the program available in Vetelino's group at the University of Maine), and then trying to build a Floquet theory on this base. It soon became clear that, to do this, it would be necessary to numerically compute the fields for each space harmonic. Since the leaky wave calculation is itself complicated and time consuming, this did not appear to be a viable method. Instead, the relatively simple direct method for calculating the height of the grating required to convert a pseudo SSBW into a true SSBW with mixed polarization was used. This method, based on the use of crystal slowness surfaces, is outlined in the following paragraph.

For simplicity, we will consider only the case of X-propagating Y-cut waves. However the program developed later in this section is completely general and can calculate grating dimension for waves on a substrate of any crystal symmetry and orientation. The Floquet theory used resembles that used for the theory for pure STW propagation normal to the X-axis on rotated Y-cut crystals, but it is more complicated. In the substrate the fields are expanded in space harmonics, and the coupled space harmonic equations are developed by means of the Datta-Hunsinger boundary condition for the grating. For pure STW, each space harmonic has only an SH polarization. For the case of quasi-STW, space harmonics of all three polarizations exist. These can be visualized on the slowness curve Fig. 14, by

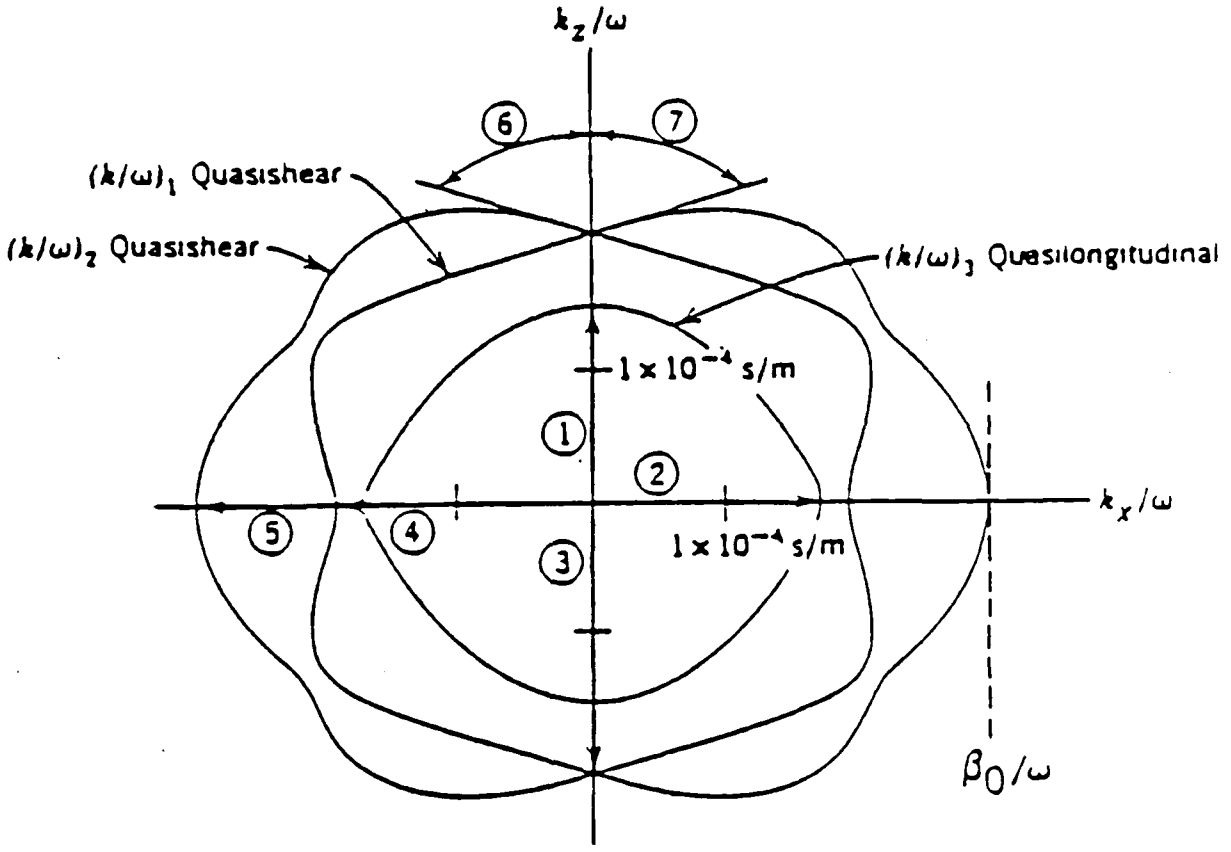

FIGURE 14

Illustrates the condition for a skimming wave on X-propagating Z-cut lithium niobate or tantalate.

taking

$$\frac{K_x}{\omega} = \frac{\beta_n}{\omega} \tag{54}$$

This allows one to visualize which space harmonics are leaky and which are not. The grating wave becomes nonleaky when β_0/ω first reaches the extremum of the slow shear wave. At this point, the 0th fast shear and longitudinal space harmonics are already nonleaky and all of the higher space harmonics are nonleaky. To calculate the height of grating required to make this a viable solution, the coupled mode approximation is made, including in this case 0th and -1th space harmonics of all three types. The grating height must then be evaluated by applying the zero determinant condition to the set of coupled equations for these six space harmonic amplitudes. In this procedure, unlike the programs developed for calculating surface wave velocities, the values of β_x/ω for the various space harmonics are obtained from the slowness curves. They do not have to be guessed by successive trials, as in numerical analysis of Rayleigh waves on a smooth surface, and can be used directly to find the field values needed in setting up the boundary condition equation for h. As in the space harmonic problems already treated, the accuracy of the coupled mode solution can be subsequently tested and improved by including additional space harmonic amplitudes.

(b) Trapping of Leaky Surface Waves

Consider plane surface wave propagation along the Z-axis of a nonpiezoelectric anisotropic crystal half space with a rotated coordinate system orientated such that the $X - Z$ plane corresponds to the surface of the half space and the Y-axis is directed into the crystal. As in the STW theory we consider a surface perturbation of this structure, in the form of a shallow surface grating that is infinite in extent and orientated normal to the direction of plane surface wave propagation. Floquet theory will be combined with the method of superposition of partial waves to solve this single crystal grating problem.

In the STW case we had a simple unperturbed wave solution consisting of a shear horizontal displacement velocity, the SH mode. Following Floquet theory, we assumed

the perturbed wave solution to consist of a summation of space harmonics, where each space harmonic is a pure SH wave at a different spatial frequency. For the more general wave solution now under consideration, we know the unperturbed wave solution can be expressed as a superposition of three partial waves (quasi longitudinal, fast quasi shear, and slow quasi shear). Following Floquet theory, we can express the perturbed solution as a sum of space harmonics, where each space harmonic is a pure unperturbed wave at a different spatial frequency. The grating wave, or perturbed wave, then has a displacement velocity solution of the form

$$v_{(y,z,t)} = \sum_{N} \left\{ a_n^L \hat{v}_n^L e^{-\alpha_n^L y} + a_n^F \hat{v}_n^F e^{-\alpha_n^F y} + a_n^S \hat{v}_n^S e^{-\alpha_n^S y} \right\} e^{-i\beta_n z} e^{i\omega t} \tag{55}$$

where

a_n^L is the amplitude of the n-th quasi-longitudinal space harmonic.
a_n^F is the amplitude of the n-th fast quasi-shear space harmonic.
a_n^S is the amplitude of the n-th slow quasi-shear space harmonic.
$\hat{v}_n^L$ is the unit displacement velocity for the quasi-longtudinal partial wave.
$\hat{v}_n^F$ is the unit displacement velocity for the fast quasi-shear. partial wave.
$\hat{v}_n^S$ is the unit displacement velocity for the slow quasi-shear partial wave.
α_n^L, α_n^F and α_n^S are the complex lateral attenuation constants for the quasi- longitudinal, fast quasi-shear, and slow quasi-shear, respectively.
β_n is the n-th space harmonic propagation constant along the Z-axis.
ω is the grating wave frequency.

The first step in finding a solution to the leaky wave problem is to find the partial wave lateral attenuation constants and displacement velocity vectors. A partial wave solution of the form described above is assumed.

$$a_n \hat{v}_n e^{-\alpha_n y} \tag{56}$$

This general partial wave solution is substituted into the acoustic wave equation,[37] neglecting the body forces F

$$\nabla \cdot c : \nabla_s v = \rho \frac{\partial^2 v}{\partial t^2} \tag{57}$$

Following an approach similar to the one used to derive the Christoffel equation for triclinic crystals,[38] the following system of linear equations relating the attenuation constants and displacement vectors to ω and β for the three partial wave solutions in Eq. 55 was found.

$$\begin{bmatrix} A & D & E \\ D & B & F \\ E & F & C \end{bmatrix} \begin{bmatrix} v_x \\ v_y \\ v_z \end{bmatrix} = 0$$

$$\begin{aligned} A &= c_{55}\beta_n^2 - c_{66}\alpha_n^2 - i2c_{56}\beta_n\alpha_n - \rho\omega^2 \\ B &= c_{44}\beta_n^2 - c_{22}\alpha_n^2 - i2c_{24}\beta_n\alpha_n - \rho\omega^2 \\ C &= c_{33}\beta_n^2 - c_{44}\alpha_n^2 - i2c_{34}\beta_n\alpha_n - \rho\omega^2 \\ D &= c_{45}\beta_n^2 - c_{26}\alpha_n^2 - i(c_{46} + c_{25})\beta_n\alpha_n \\ E &= c_{35}\beta_n^2 - c_{46}\alpha_n^2 - i(c_{45} + c_{36})\beta_n\alpha_n \\ F &= c_{34}\beta_n^2 - c_{24}\alpha_n^2 - i(c_{44} + c_{23})\beta_n\alpha_n \\ c_{ij} &= \text{ the rotated stiffness constants.} \end{aligned} \tag{58}$$

Using numerical methods, this set of liner equations can be solved for the six complex values of α_n, given β_n. We then select the three lateral attenuation constants values that correspond to surface wave solutions (i.e., those solutions which go to zero when Y is infinite). These three values correspond to α_n^L α_n^F, and α_n^S in Eq. 55.

These solutions are an extension of the slowness surface calculation.[39] If the lateral attenuation constants are restricted to be pure imaginary (corresponding to wave propagation constants that are pure real) the solution to the above system of equations would result in the crystal slowness surfaces discussed in the literature.[39] This allows for a check of the numerical program by selecting wave velocities that are greater than the slowest shear wave and then comparing the solutions with the corresponding crystal slowness surface discussed in the literature. In general, the lateral attenuation constants can be complex, corresponding to wave propagation with attenuation.

Once the three partial wave attenuation constants have been found, then they can be substituted into Eq. 58 to find the corresponding particle displacement velocity vectors

$[v_x, v_y, v_z]$. In general, these velocity vectors are complex and the numerical computation must allow for this possibility, as well as for possible pure mode displacement velocity vectors.

Using the algorithm described above, three partial wave lateral attenuation constants and displacement vectors can be found for each space harmonic, once the crystal orientation and wave velocity have been specified. That is to say, if the numerical values for the wave frequency ω, the propagation constant β_0, crystal density ρ and the crystal stiffness values c_{IJ} are known, then the three partial wave lateral attenuation constants and the three particle displacement velocity vectors can be determined. This partial wave calculation is then repeated for each space harmonic propagation constant β_n. These partial wave solutions can now be used to solve the boundary condition equation at the surface of the substrate.

The partial wave amplitudes of each individual space harmonic must be selected so that the boundary condition at the surface of the half space is satisfied. In the general geometry, Datta-Hunsinger boundary condition equations, including all three polarization displacements, are applied. As in the STW case, this gives coupled space harmonic equations; but, unlike the STW case, there are now three scalar equations corresponding to each space harmonic. Using the orthogonality properties of the space harmonics and the Datta-Hunsinger boundary conditions, as was done in the STW case, the three following coupled space harmonic equations were found

$$a_q^L \psi_q^{2L} + a_q^F \psi_q^{2F} + a_q^S \psi_q^{2S} = \frac{h}{\Lambda} \sum_n a_n^L K_{nq}^{4L} + a_n^F K_{nq}^{4F} + a_n^S K_{nq}^{4S} \qquad (59a)$$

$$a_q^L \psi_q^{4L} + a_q^F \psi_q^{4F} + a_q^S \psi_q^{4S} = \frac{h}{\Lambda} \sum_n a_n^L K_{nq}^{3L} + a_n^F K_{nq}^{3F} + a_n^S K_{nq}^{3S} \qquad (59b)$$

$$a_q^L \psi_q^{6L} + a_q^F \psi_q^{6F} + a_q^S \psi_q^{6S} = \frac{h}{\Lambda} \sum_n a_n^L K_{nq}^{5L} + a_n^F K_{nq}^{5F} + a_n^S K_{nq}^{5S} \qquad (59c)$$

where

$$\psi_q^{IJ} = \left\{ [c_{I6}\alpha_q^J + ic_{I5}\beta_q]\hat{v}_x^J + [c_{I2}\alpha_q^J + ic_{I4}\beta_q]\hat{v}_y^J + [c_{I4}\alpha_q^J + ic_{I3}\beta_q]\hat{v}_z^J \right\}$$

$$K_{nq}^{IJ} = \frac{i\Lambda}{2}\left[G_n^{IJ}\beta_n - i\omega^2\rho'\hat{v}_{\ell n}^J \right] \qquad n = q$$

$$K_{nq}^{IJ} = \left[\frac{1-\cos\pi(n-q)}{\beta_b - \beta_q} \right]\left[G_n^{IJ}\beta_q - i\omega^2\rho'\hat{v}_{\ell n}^J \right] \quad n \neq q$$

$$\ell = x, y, z \quad \text{for} \quad I = 5, 4, 3$$

$$G_n^{IJ} = [(c'_{I6}\alpha_n^J + i\beta_n c'_{I5})v_{xn}^J + (c'_{I2}\alpha_n^J + i\beta_n c'_{I4})v_{yn}^J + (c'_{I4}\alpha_n^J + i\beta_n c'_{I3})v_{zn}^J]$$

In the previous analyses slow (or surface) wave solutions occurring below the first stopband of the grating are calculated, in the weak grating approximation, by assuming all but the 0th and -1th space harmonic amplitudes to be of negligible amplitude. The infinite set of coupled space harmonic equations Eq. 59 is then reduced to six linear equations with the following characteristic determinant.

$$\begin{bmatrix} \chi_{00}^{2L} & \chi_{00}^{2F} & \chi_{00}^{2S} & \chi_{-10}^{4L} & \chi_{-10}^{4F} & \chi_{-10}^{4S} \\ \chi_{00}^{4L} & \chi_{00}^{4F} & \chi_{00}^{4S} & \chi_{-10}^{3L} & \chi_{-10}^{3F} & \chi_{-10}^{3S} \\ \chi_{00}^{6L} & \chi_{00}^{6F} & \chi_{00}^{6S} & \chi_{-10}^{5L} & \chi_{-10}^{5F} & \chi_{-10}^{5S} \\ \chi_{0-1}^{4L} & \chi_{0-1}^{4F} & \chi_{0-1}^{4S} & \chi_{-1-1}^{2L} & \chi_{-1-1}^{2F} & \chi_{-1-1}^{2S} \\ \chi_{0-1}^{3L} & \chi_{0-1}^{3F} & \chi_{0-1}^{3S} & \chi_{-1-1}^{4L} & \chi_{-1-1}^{4F} & \chi_{-1-1}^{4S} \\ \chi_{0-1}^{5L} & \chi_{0-1}^{5F} & \chi_{0-1}^{5S} & \chi_{-1-1}^{6L} & \chi_{-1-1}^{6F} & \chi_{-1-1}^{6S} \end{bmatrix} \begin{bmatrix} a_0^L \\ a_0^F \\ a_0^S \\ a_{-1}^L \\ a_{-1}^F \\ a_{-1}^S \end{bmatrix} = 0 \qquad (60)$$

where

$$\chi_{00}^{IJ} = \psi_0^{IJ} - \frac{h}{\Lambda}K_{00}^{\ell}$$

$$\chi_{-1-1}^{IJ} = \psi_-^{IJ}1 - \frac{h}{\Lambda}K_{-1-1}^{\ell}$$

$$\chi_{-10}^{IJ} = -\frac{h}{\Lambda}K_{-10}^{IJ}$$

$$\chi_{0-1}^{IJ} = -\frac{h}{\Lambda}K_{0-1}^{IJ}$$

$$I = 1, 2, 3, 4, 5, 6$$

$$\ell = 4, 3, 5 \text{ for } I = 2, 4, 6, \text{ respectively}$$

$$J = L, F, S$$

Numerical methods were used to solve for the height-to-period ratio which satisfies Eq. 60 at a specified wave velocity and crystal orientation—that is, for specified ω, β, crystal stiffness constants and crystal density. This height-to-period ratio corresponds to the theoretical grating dimensions needed to trap the leaky wave, or in the case of a non-leaky wave, the grating dimensions required to slow the surface wave velocity to the velocity specified.

Equation (60) given above is of sixth order in the height-to-period ratio, and therefore has six different solutions. If more space harmonics were included, there would be a corresponding increase in the number of roots to the equation. Roots giving a real positive height-to-period ratio correspond to the physical grating dimensions that would slow the wave to the velocity specified in the program. If that velocity is slower than the slowest bulk wave, then the wave is a trapped surface wave as described above. Complex roots are not physically realizable, and must be regarded as spurious. In cases where none of the six roots are real and positive, then the wave velocity specified at the beginning of the numerical calculation cannot be achieved with a physical grating. However, if there is at least one positive real root (or, in some cases, more than one) then these correspond to grating heights that trap leaky waves at the specified velocity and crystal orientation.

(c) Numerical Results

A Fortran program based on the above algorithm has been developed and tested. The program calculates the grating height-to-period ratio needed to slow a leaky wave to a specified wave velocity. If the prespecified wave velocity is less than the slowest shear bulk wave velocity found from the slowness surface, then the grating height-to-period ratio found corresponds to one that will trap a leaky wave. The program can consider arbitrary crystal cuts and propagation directions but neglects piezoelectricity. Neglecting piezoelectricity sometimes can present a problem when comparing the results to other published calculations of leaky waves on smooth surfaces. These published results included the piezoelectric effect in the higher coupling materials considered (lithium niobate and lithium tantalate) because the piezoelectrical effect can change the wave velocity on the

order of 20%. To make completely accurate comparisons, the piezoelectrical potential terms will have to be incorporated into the program in the future.

The program was applied to the problem of wave propagation along the X-axis of Y-cut trigonal crystal half spaces of quartz, lithium niobate and lithium tantalate. The real positive height-to-period ratio needed to trap the leaky waves or slow existing surface waves was calculated for various assumed wave velocities. There are four major wave velocity regions, two of which are of primary interest. Region One has wave velocities greater than the slow bulk shear wave velocity. Region Two has wave velocities greater than the SAW velocity, but less than the slow bulk shear wave velocity. Region Three has wave velocities less than the SAW velocity, but greater than the minimum trapped wave velocity. Finally, Region Four has wave velocities less than the minimum trapped wave velocity.

In Region One the program fails to find any roots because some of the partial wave lateral attenuation constants needed in the partial wave solution are pure-imaginary. The program bases its selection of the three attenuation constants α on the sign of the real parts of the α's. If the real part of any α is zero, then the program rejects the initially chosen velocity, because lateral attenuation constants suitable for trapped leaky waves require roots with a positive real part.

In Regions Two and Three, the real parts of the α's are non-zero and the height-to-period ratio is found to have real positive roots. These are the areas of major interest and they have been plotted for wave propagation along the X-axis of Y-cut crystal half spaces of quartz, lithium niobate, and lithium tantalate in Figs. 15, 16, 17, and 18. In each case there exists a grating SAW solution and a trapped leaky wave solution. The grating SAW has a real positive height-to-period ratio that descends from infinity, at the minimum trapped wave velocity, to a value of zero, at the wave velocity corresponding to the SAW velocity on a smooth surface, neglecting piezoelecticity. The trapped leaky wave has a height-to-period ratio that descends from infinity, at the minimum trapped leaky wave velocity, to a minimum height-to-period ratio needed to trap the leaky wave. This minimum height-to-period ratio needed to trap the leaky wave is the height-to-period

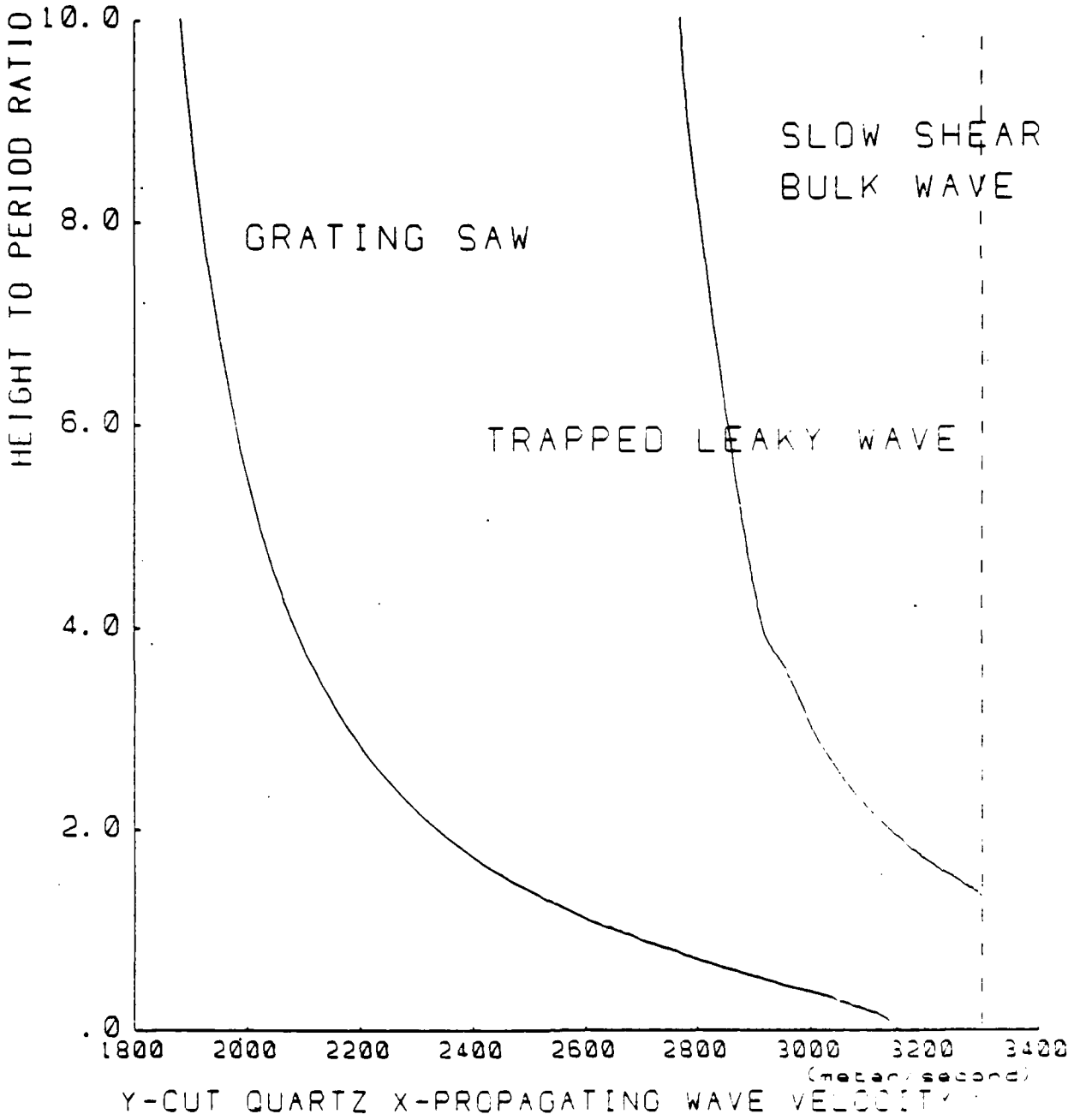

FIGURE 15

Real height-to-period ratio needed to trap leaky wave and SAW propagating along the X-axis of Y-cut quartz.

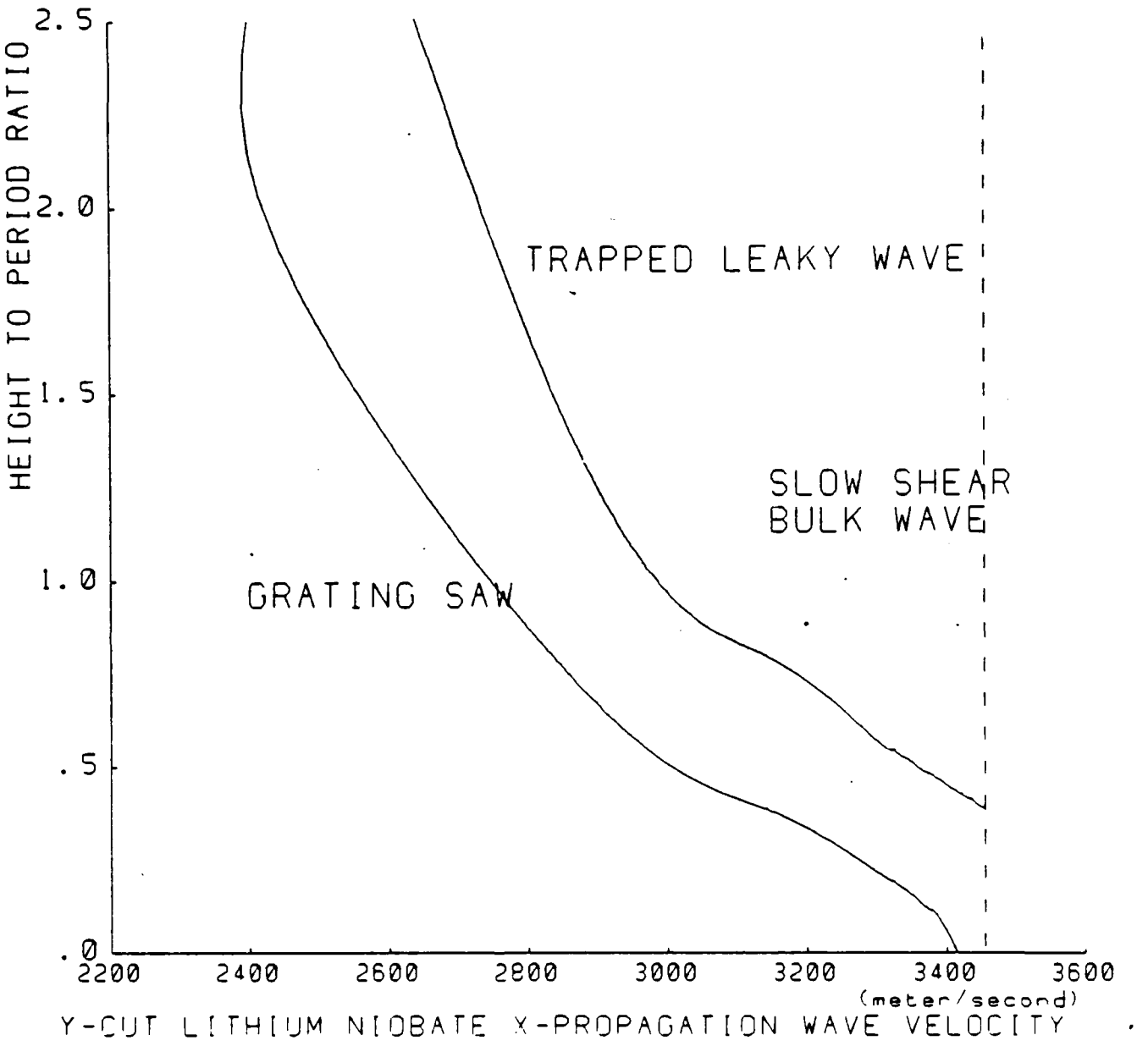

FIGURE 16

Real height-to-period ratio needed to trap leaky wave and SAW propagating along the X-axis of Y-cut lithium niobate.

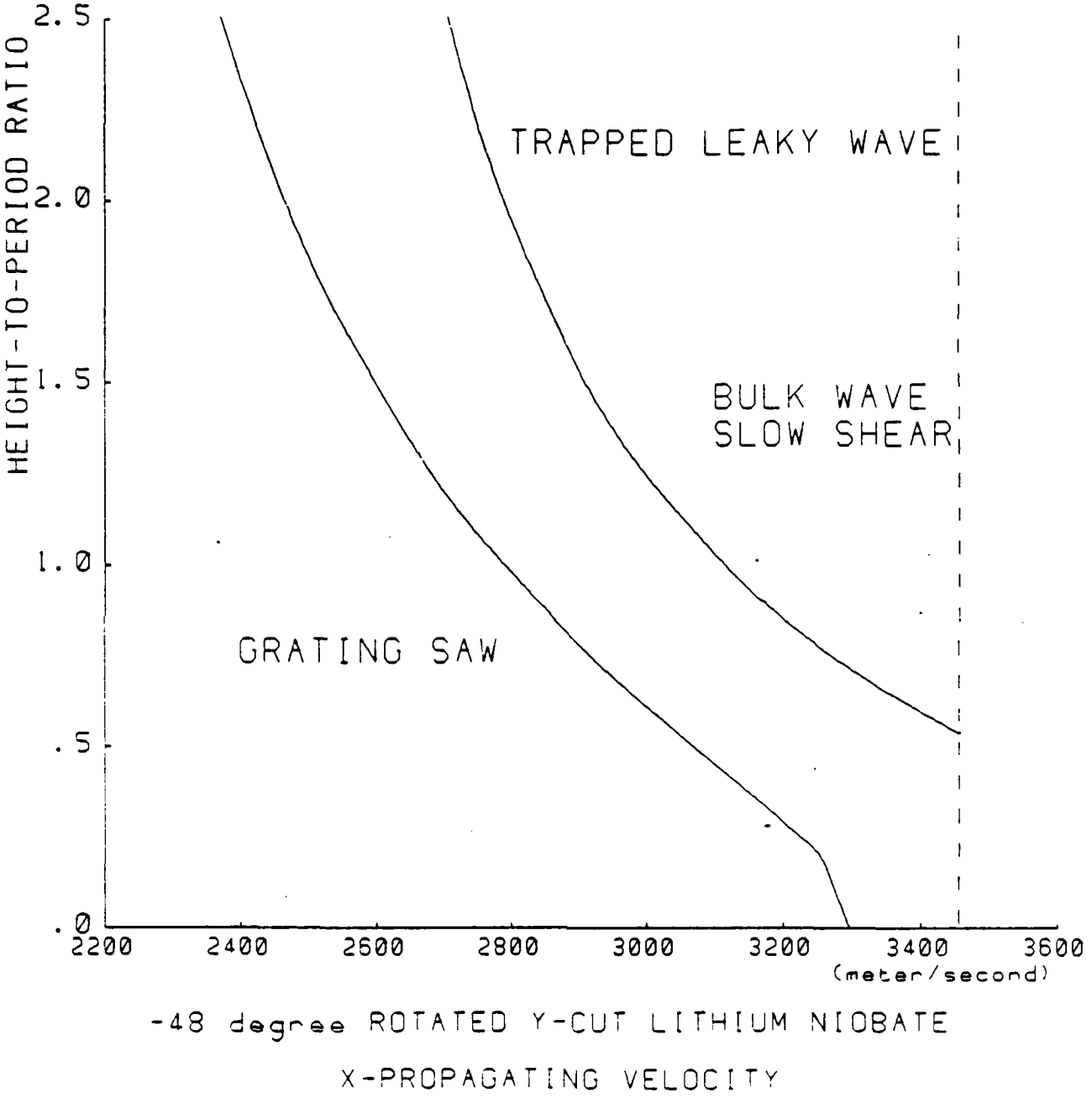

FIGURE 17

Real height-to-period ratio needed to trap leaky wave and SAW propagating along the X-axis of -48° rotated Y-cut (maximum coupling $\Delta v/v = 0.02775$).

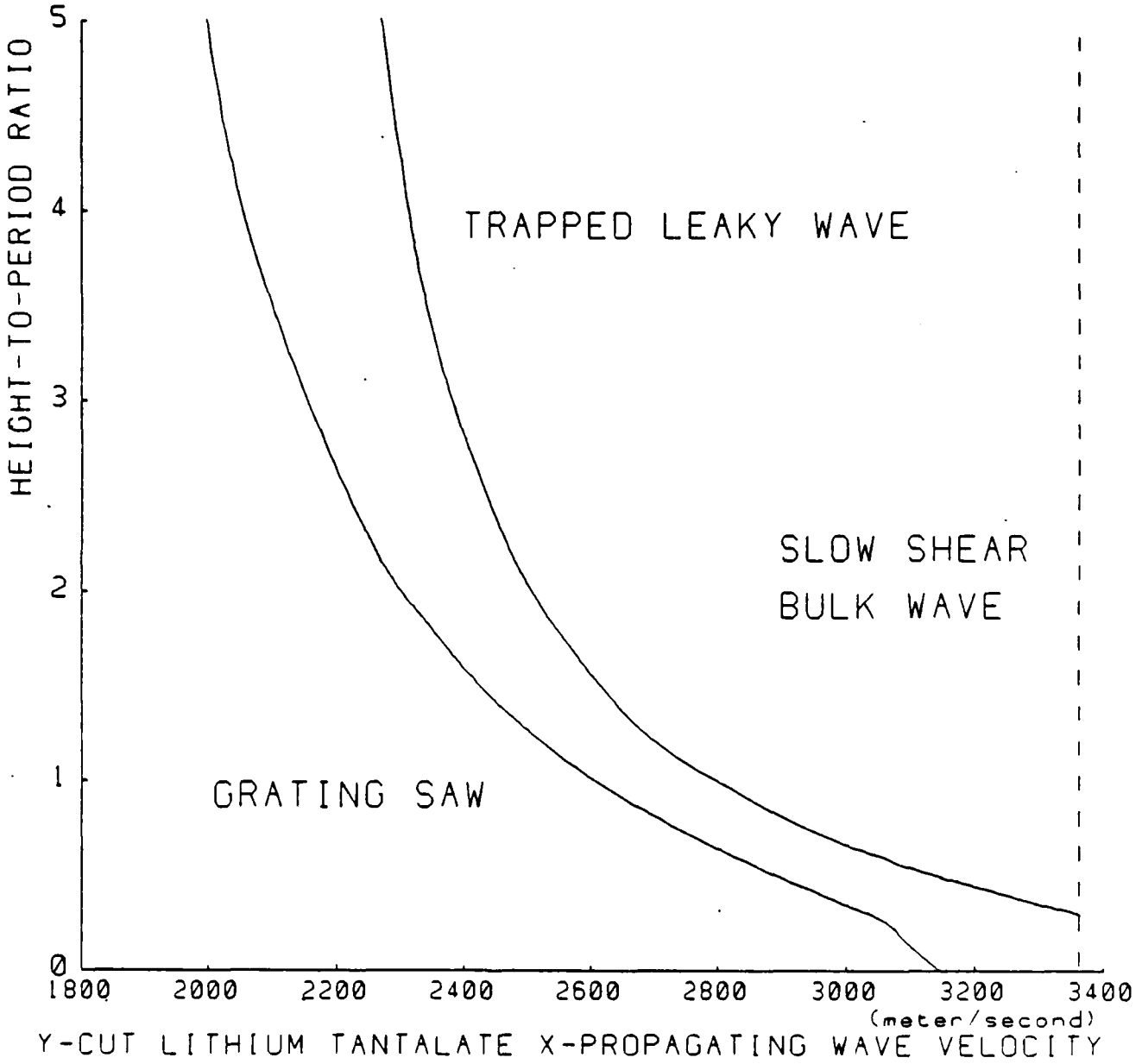

FIGURE 18

Real height-to-period ratio needed to trap leaky wave and SAW propagating along the X-axis of Y-cut lithium tantalate.

ratio needed to slow the leaky surface wave velocity, which is greater than the slow shear bulk wave velocity (and thus leaky) to the slow shear bulk wave velocity where it become a surface skimming wave. When the grating height is increased beyond this minimum, the surface skimming wave becomes a trapped leaky wave.

In Region Four, the prespecified wave velocity is so slow that there are no real positive height-to-period ratios that can slow the leaky wave to the specified velocity. Because no real roots are present in this region it is not of interest for trapped leaky wave analysis and will not be discussed further.

These encouraging results show that the grating dimensions needed to trap leaky waves can be calculated using the algorithm developed. However, the minimum grating height-to-period ratios needed to trap X-propagating leaky waves on Y-cut crystals are relatively large (quartz $h/\Lambda = 1.3$; lithium niobate $h/\Lambda = 0.38$; lithium tantalate $h/\Lambda = 0.29$). This is the same as the problem encountered in normal mode SAGW theory, where the large height-to-period results were questioned because of the shallow grating assumption made in the Datta-Hunsinger boundary conditions. The gratings found here are not as deep as those found earlier, but are still in the range where the Datta-Hunsinger assumptions are in question. Any attempt to add additional grating height to temperature compensate these trapped leaky waves would result in grating depths contradicting the Datta-Hunsinger assumption.

To alleviate the deep grating problem described above the program was used to locate crystal orientations where trapped leaky waves can be supported with shallow gratings. The orientations considered are propagation along the X-axis of rotated Y-cut quartz, lithium niobate, and lithium tantalate crystal half spaces. The prespecified wave velocity used in the program is the slow shear bulk wave velocity, which gives the grating height-to-period ratio needed to turn the leaky wave into a surface skimming wave. These height-to-period ratios are plotted as a function of crystal rotation angle for quartz, lithium niobate, and lithium tantalate in Figs. 19, 20 and 21.

In lithium tantalate there is only one real positive root for the grating height-to-period ratio needed to turn the leaky wave into a skimming wave. The grating height goes to

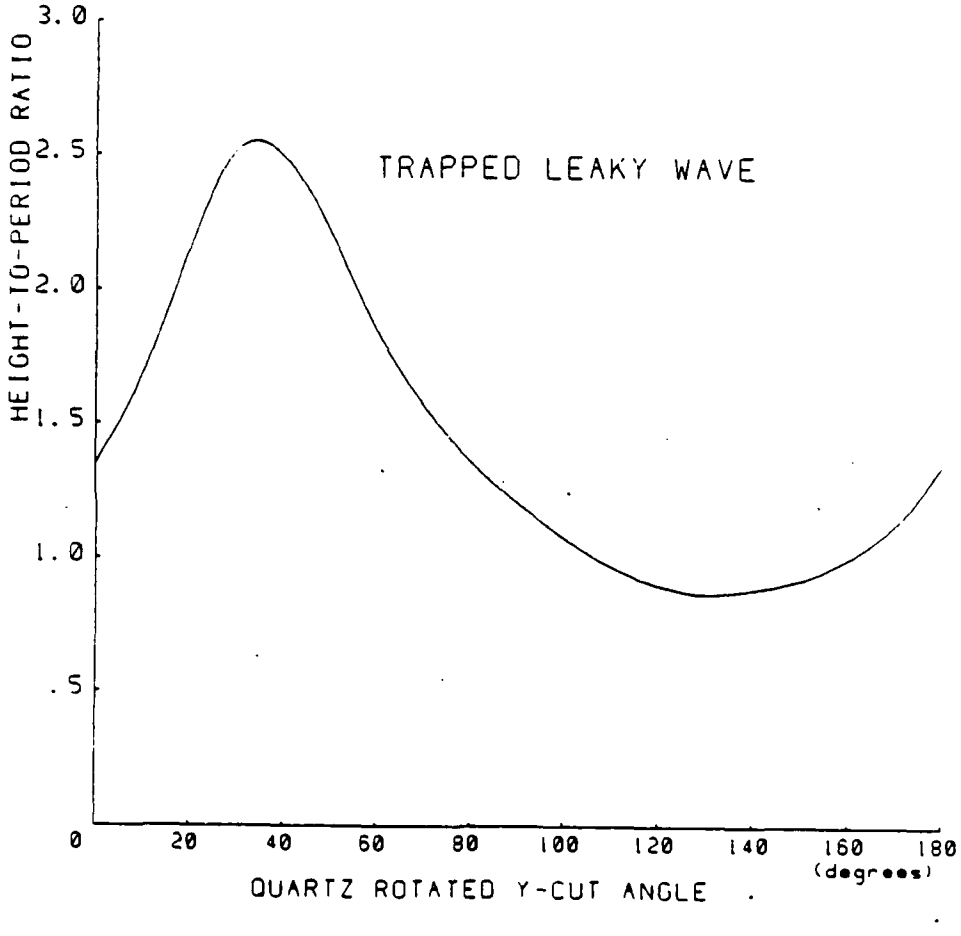

FIGURE 19

Height-to-period ratio needed for surface skimming wave propagation on rotated Y-cut quartz.

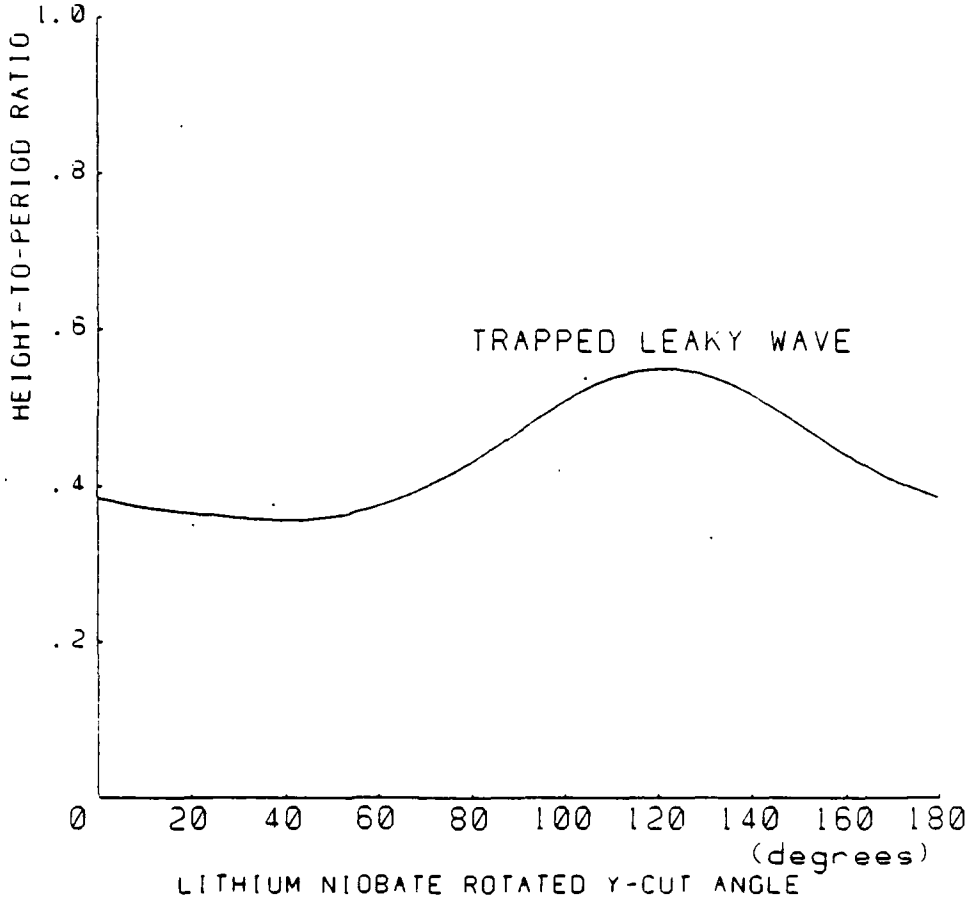

FIGURE 20

Height-to-period ratio needed for surface skimming wave propagation on rotated Y-cut lithium niobate.

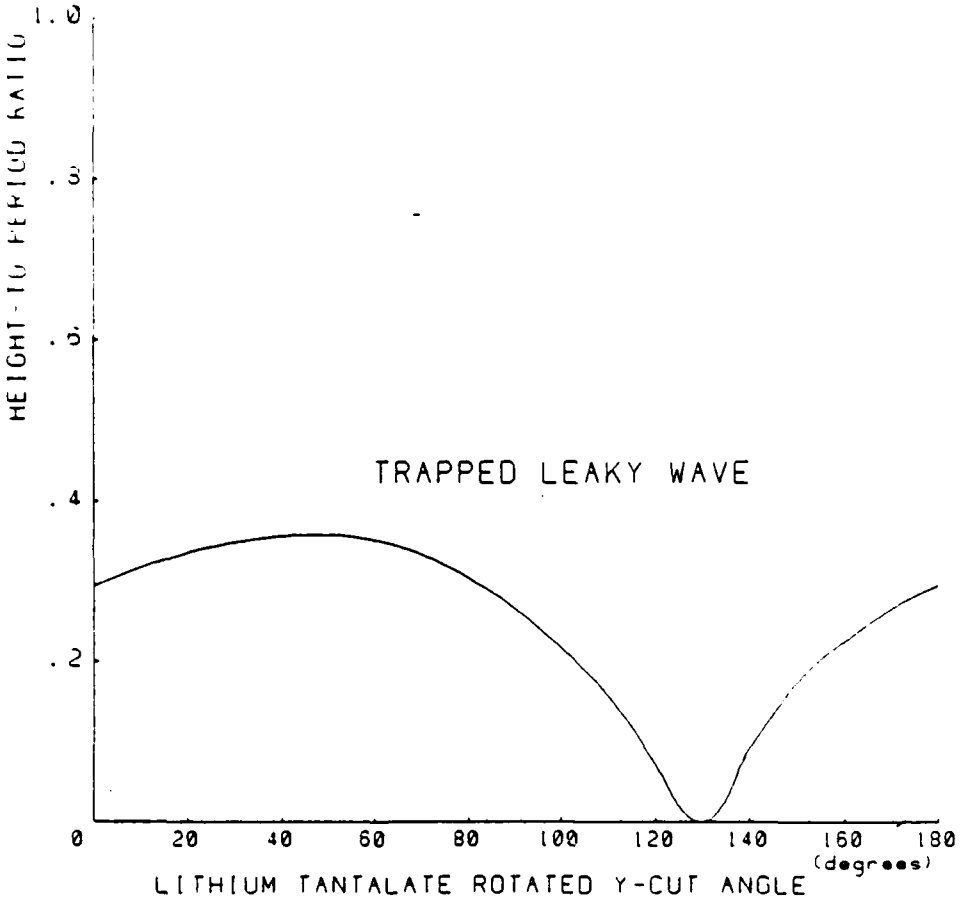

FIGURE 21

Height-to-period ratio needed for surface skimming wave propagation on rotated Y-cut lithium tantalate.

zero over a short range of Y−cut angles near 130°. This angle corresponds to the surface skimming wave reported in the literature[22] (Note: The angle quoted in the literature, calculated using the piezoelectric potential, is 125°; the angle found here, neglecting piezoelectricity, is 130°.) The grating dimensions near this rotated Y-cut correspond to those of a shallow grating and are accurately predicted with this leaky wave theory. The grating height can be increased to trap the skimming wave and thereby create a surface grating wave on lithium tantalate. This type of surface wave has the high coupling of lithium tantalate and also temperature characteristics that are a function of the grating dimensions.

In the case of quartz and lithium niobate there are no rotated Y-cut angles found that can trap a leaky wave with a grating height-to-period ratio less than 0.4. Because of the deep grating problems described above, the temperature compensation investigation of trapped leaky waves on these materials is open to question. However, with the piezoelectric effect included in the program, there may be an additional solution that may allow for trapping with shallow gratings. To develop this computation would require a piezoelectric counterpart of the Datta-Hunsinger equations.

The above analysis demonstrates the need for further work in this area. It already shows that gratings can, in principle, be used to trap leaky surface acoustic waves, but a more refined theory will be required for quantitative grating design of sufficient accuracy for devices. Such a further development would permit a systematic evaluation of piezoelectric coupling and temperature compensation in trapped leaky waves for all doubly-rotated crystal cuts. Since some leaky waves are already known to have very large piezoelectric coupling, such an evaluation could well yield new crystal cuts providing optimized combinations of high coupling and temperature compensation for surface wave delay lines.

VI. CONCLUSION

The original and modified goals of this project are repeated here to provide a perspective for this brief summary and interpretation of the results detailed above:

(a) Original Goals

The technical objective of this research was to further develop the theory of horizontally-polarized shear surface wave propagation on surfaces having periodic mechanical or electrical loading (surface transverse waves, STW), with special reference to their temperature- and stress-compensation properties.

(i) Work statement for first 12-month period

Task 1 Develop and evaluate for various materials a temperature perturbation analysis of TCD for grooved STW on rotated Y-cut trigonal crystals.

Task 2 Make a quantitative estimate of the degree of temperature compensation achievable with a grooved structure, to determine the likelihood of achieving zero temperature coefficient with choice of groove shape only.

(ii) Work statement for second 12-month period

Task 3 Look for temperature compensated gratings (involving grooves, mass loading and conduction effects) for $LiNbO_3$ and $LiTaO_3$.

Task 4 Develop a theory of conducting strip STW theory for planar surfaces of rotated Y-cut trigonal crystals and evaluate for various materials.

Task 5 Adapt Task 1 to mass loading STW.

Task 6 Develop theory of grooved STW to include complete and partial conductive coatings on rotated Y-cut trigonal crystals.

Task 7 Develop theory of grooved plus mass loading STW.

Task 8 Perform Task 3 in more detail.

(b) Modified Goals

In the second year of the program it was decided that the STW restriction is much too limited, because very few crystal cuts exhibit this type of solution. Restriction to these

cuts eliminates many useful substitutes, such as the high coupling X-propagating rotated Y-cuts of lithium niobate and lithium tantalate. On these cuts important leaky surface waves exist and have already been used to some extent in devices reported in the literature. For this reason the goals were extended as follows:

Task 9 Develop a generalized grating wave theory for both SAW and leaky grating waves on arbitrary crystal cuts.

Task 10 Use the generalized theory to develop a procedure for trapping a leaky surface wave by means of a surface grating of appropriate design.

Task 11 Examine the temperature compensation properties of trapped leaky surface waves.

(c) Tabulated Results and Recommendations

- Grooved grating temperature compensation demonstrated theoretically for STW (propagation to X on rotated Y-cut substitutes) in quartz, lithium niobate and lithium tantalate.
- STW temperature compensated theory extended to mass loading gratings.
- Static strain effects characterized and evaluated for mass loading gratings—a dominant effect.
- Electrical conduction grating effects on temperature compensation shown to be much smaller than other effects, even in high coupling materials.
- Normal mode theory of Rayleigh grooved grating waves (SAGW) developed and applied to X-propagation rotated Y-cuts—deep gratings required for compensation.
- Novel trapped leaky wave grating algorithm developed for arbitrary crystal cuts, ignoring piezoelectricity.
- Leaky wave trapping calculations made for X-propagating rotated Y-cut quartz, lithium niobate and lithium tantalate—modest to small grating heights required for niobate and tantalate.

- Observed that trapped leaky wave theory must be extended to include piezoelectricity, before meaningful temperature compensation calculations can be made.

REFERENCES

1. B. A. Auld, J. J. Gagnepain, and M. Tan, *Electron. Lett* **12**, pp. 650–651 (1976).
2. B. A. Auld, A. Renard, and J. Henaff, *Electron. Lett.* **18**, pp. 183–184 (1981).
3. D. A. Watkins, *Topics in Electromagnetic Theory*, (John Wiley & Sons, New York, 1958), pp. 14–19.
4. R. M. Bevensee, *Electromagnetic Slow Wave Systems*, (John Wiley & Sons, New York, 1964), pp. 57–61.
5. A. Renard, J. Henaff, and B. A. Auld, 1981 *IEEE Ultrasonics Symposium Proceeings*, pp. 123–128.
6. B. A. Auld and B. H. Yeh, 1979 *IEEE Ultrasonics Symposium Proceedings*, pp. 786–790.
7. C. Elachi, *Proceedings of the IEEE*, **64**, pp. 1666–1698 (1976).
8. S. Datta and B. J. Hunsinger, *J. Appl. Phys.* **50**, pp. 5561–5665 (1979).
9. G. Cambon, J. M. Surel, J. Lassale, J. Attal, and W. Shahab, 1981 *Ultrasonics Symposium Proceedings*. pp. 364–367.
10. R. T. Smith and J. S. Welsh, *J. Appl. Phys.* **42**, pp. 2219–2230 (1971).
11. R. Bechmann, A. D. Ballato, T. J. Lukaszek, *Proc. IRE* **50**, pp. 1812–1822 (1962).
12. M. Lewis, 1977 *IEEE Ultrasonics Symposium Proceedings*, pp. 744–752.
13. K. H. Yen, K. F. Lau, and R. S. Kagiwada, 1979 *IEEE Ultrasonics Symposium Proceedings*, pp. 776–786.
14. R. Lec, J. F. Vetelino, F. Josse, D. S. Bailey, and M. Ehsasi, 1980 *IEEE Ultrasonics Symposium Proceedings*, pp. 424–428.
15. R. N. Thurston, H. J. McSkimin, and P. Andreatch, Jr., *J. Appl. Phys.* **37**, pp. 267–275 (1966).
16. K. Burgger, *J. Appl. Phys.* **36**, pp. 759–768 (1965).
17. Y. Nakagawa, K. Yamanouchi, and K. Shibayama, *J. Appl. Phys.* **44**, pp. 3969–3974.
18. A. L. Nalmwar and M. Epstein, *J. Appl. Phys.* **47**, pp. 43–48 (1976).
19. P. L. Castro and J. F. Campbell, *Ohmic Contacts to Semiconductors*, Bertram Schwartz, ed., (The Electrochemical Society, Inc., New York, 1969), pp. 332–338.

20. S. Elliott and R. Bray, Private Communication (1985).

21. P. H. Carr, A. Jhunjhunwala, L. A. Veilleux, J. F. Vetelino, and J. C. Field, 1977 *IEEE Ultrasonics Symposium Proceedings*, pp. 679–682.

22. K. Nakamura, M. Kazumi, and H. Shimizu, 1977 *IEEE Ultrasonics Symposium Proceedings*, pp. 819–822.

23. D. Chang, Y. A. Shui, and W. H. Jiang 1982 *IEEE Ultrasonics Symposium Proceedings*, pp. 53–56.

24. A. Renard, J. Henaff, and B. A. Auld, 1981 *IEEE Ultrasonics Symposium Proceedings*, pp. 123–128.

25. A. J. Slobodnik and E. C. Conway, *Microwve Acoustics Handbook*, (Office of Aerospace Research, USAF, 1970).

26. J. Andle, Private Communication (1985).

27. R. Bechmann, A. D. Ballato, and T. J. Lukaszek, *Proc. IRE*, **50**, pp. 1812–1822 (1962).

28. R. T. Smith and J. S. Welsh, *J. Appl. Phys.* **42**, pp. 2219–2230 (1971).

29. B. A. Auld, *Acoustic Fields and Waves in Solids, Vol. II*, (Wiley-Interscience, New York, 1973); pp. 286–290.

30. B. A. Auld, *Acoustic Fields and Waves in Solids, Vol. II*, (Wiley-Interscience, New York, 1973); pp. 306–307.

31. K. Blotekhaer, K. A. Ingebrigtsen, and H. Skeie, *IEEE Trans. on Electron Devices* **20**, pp. 1139–1147 (1973).

32. J. B. Davies, *Electron. Lett.* **20**, pp. 720–722 (1984).

33. A. Takayanagi, K. Yamanouchi, and K. Shibayama, *Appl. Phys. Lett.* **17**, pp. 225–227 (1970).

34. P. D. Bloch, N. G. Doe, E. G. S. Paige, and M. Yamaguchi, 1983 *Ultrasonics Symposium Proceedings*, pp. .

35. T. C. Lim and G. W. Farnell, *J. Appl. Phys.* **39**, pp. 4319–4325 (1968).

36. G. W. Farnell, "Properties of Elastic Surface Waves," Chapter 3 in *Physical Acoustics 6*, W. P. Mason and R. W. Thurston, eds., (Academic Press, New York, 1970).

37. B. A. Auld, *Acoustic Fields and Waves in Solids, Vol. I* (Wiley-Interscience, New York, 1973); p. 164.

38. B. A. Auld, *Acoustic Fields and Waves in Solids, Vol. I* (Wiley-Interscience, New York, 1973); pp. 210–212.

39. B. A. Auld, *Acoustic Fields and Waves in Solids, Vol. I* (Wiley-Interscience, New York, 1973); pp. 390–393.

40. K. Y. Hashimoto, M. Yamaguchi, and H. Kogo, 1983 *IEEE Ultrasonics Symposium Proceedings*, pp. 345–349.

41. B. A. Auld, *Acoustic Fields and Waves in Solids, Vol. II*, (Wiley-Interscience, New York, 1973); pp. 205–206.

42. B. A. Auld, *Acoustic Fields and Waves in Solids, Vol. II*, (Wiley-Interscience, New York, 1973); p. 307.

43. B. A. Auld, *Acoustic Fields and Waves in Solids, Vol. II*, (Wiley-Interscience, New York, 1973); p. 291.

44. R.L. Rosenberg, C. Chamzas, and D.A. Fishman, *IEEE Journal on Selected Areas in Communications* **SAC–2**, pp. 957–965 (1984).

APPENDIX 1

CALCULATION OF THE NORMAL MODE SPACE HARMONIC EQUATION COUPLING TERMS USED IN EQ. 39.

(1) Start with the coupling term in the space harmonic Eq. (38) using Rayleigh wave modes ($\mu = \nu = R$) and note that, for Rayleigh wave modes, $v_x = 0$

$$K_{mR,nR} = \int_0^{\Lambda} \frac{ie^{i(\beta_m - \beta_n)z}}{\Lambda U_{mR,nR}} \left[v^*_{y_{mR}} T_{yy_{mR}} + v^*_{z_{mR}} T_{zy_{nR}} \right]_{y=0} dz \qquad \text{(A1)}$$

$$\beta_m = \beta_0 + \frac{2\pi m}{\Lambda}$$

$$\beta_n = \beta_0 + \frac{2\pi m}{\Lambda}$$

(2) Recall from Reference 41 that the average stored energy per unit length in the n-th space harmonic is given by

$$U_{mR,nR} = \frac{4P_{avg}}{V_R} \tag{A2}$$

where P_{avg} is the average power in the Rayleigh wave per unit width, and V_R is the Rayleigh wave phase velocity.

(3) Further, recall the Datta-Hunsinger relation for T_{yy} and T_{yz} of the n-th space harmonic

$$T_{yy_n} = j\omega\rho h v_{y_n} \tag{A3}$$

$$T_{yz_n} = j\omega\rho h v_{z_n} - h\frac{\partial T_{zz_n}}{\partial z} \tag{A4}$$

(4) Note that h and T_{zz_n} are zero between the grating teeth ($\Lambda/2 < z < \Lambda$) and nonzero under a tooth ($0 < z < \Lambda/2$). Because of this, the following expression can be found for T_{yz_n} where the delta functions come from the derivative of T_{zz_n} at the edges of the grating teeth.

$$T_{yz_n} = j\omega\rho h\, v_{z_n} + jh\beta_n T_{zz_n} - hT_{zz_n}\left[\delta(z) - \delta\left(z - \frac{\Lambda}{2}\right)\right]$$

(5) Note that the shallow grating assumption states that the stress fields in the grating teeth are the same as those in the substrate. Therefore, using the acoustic field equations in the substrate with a z displacement, the stress T_{zz} is found to be

$$T_{zz_n} = -\frac{\rho\omega v_{z_n}}{\beta_n}$$

Substituting into Eq. (A4), T_{zy} gives

$$T_{zy_n} = \frac{\omega}{\beta_n}\rho h v_{z_n}\left[\delta(z) - \delta\left(z - \frac{\Lambda}{2}\right)\right] \tag{A5}$$

(5) Substitute Eqs. (A2), (A3), and (A5) into Eq. (A1), giving

$$K_{mR,nR} = \frac{i\omega\rho h V_R}{4\Lambda P_{avg}} \int_0^{\Lambda/2} \left[iv_{y_m}^* v_{y_n} + \frac{v_{z_m}^* v_{z_n}}{\beta_n}(\delta(z) - \delta(z-1))\right] e^{i(\beta_m - \beta_n)z} dz \tag{A6}$$

and perform the integration, giving

$$K_{mR,nR} = \begin{cases} -\frac{\omega\rho h V_R}{8}\frac{v_{y_m}^* v_{y_n}}{P_{avg}} & m = n \\ \frac{i\omega\rho h V_R}{4\Lambda P_{avg}}[1 - \cos\pi(m-n)]\left[-\frac{v_{y_m}^* v_{y_n}}{\frac{2\pi}{\Lambda}(m-n)} + \frac{v_{z_m}^* v_{z_n}}{\beta_n}\right] & m \neq n \end{cases}$$

(7) Make the near resonance approximation

$$\begin{aligned} m &= 0, -1 \\ n &= 0, -1 \\ \omega/\beta &= V_R \\ \beta_0 &= \pi/\Lambda \\ \beta_{-1} &= -\pi/\Lambda \end{aligned}$$

(8) Note that the relation between the forward wave and reverse wave particle displacement velocities is (from Ref. 42)

$$V_{R-} = -V_{R+}^*$$

and that the particle displacements normalizations used in the SAW data are

$$\frac{v_{y_m}^* v_{y_n}}{P_{avg}} = \omega \frac{U_{y_m}^* U_{y_n}}{P_r}$$

This leads to the relation for the coupling terms appearing in Eq. (39)

$$\begin{aligned} K_{00} = K_{-1-1} &= -\frac{\rho\pi^2 V_R^3}{8\Lambda}\left(\frac{h}{\Lambda}\right)\frac{|U_y|^2}{P_r} \\ K_{0-1} = K_{-10}^* &= \frac{i\rho\pi}{4\Lambda} V_R^3 \left(\frac{h}{\Lambda}\right)\left[\frac{(U_y^*)^2}{P_r} + \frac{2(U_z^*)^2}{P_r}\right] \end{aligned} \qquad (A7)$$

APPENDIX 2

DERIVATION OF THE SURFACE ACOUSTIC GRATING WAVE VELOCITY EQ. (40) FROM THE NEAR STOP-BAND COUPLED WAVE EQUATION EQ. (39)

Recall that the near stop-band coupled wave equation (Eq. (39)) in matrix form is

$$\begin{bmatrix} \omega - V_R\beta_0 - K_{00} & -K_{0-1} \\ -K_{-10} & \omega + V_R\beta_{-1} - K_{-1-1} \end{bmatrix} \begin{bmatrix} a_0 \\ a_{-1} \end{bmatrix} = 0 \qquad (A8)$$

The condition for a nontrivial solution for a_0 and a_{-1} is that the determinant of the matrix is zero. Setting the determinant equal to zero gives the following characteristic equation

$$[\omega - V_R\beta_0 - K_{00}][\omega + V_R\beta_{-1} - K_{-1-1}] - K_{0-1}K_{-10} = 0 \qquad (A9)$$

where $\beta_{-1} = \beta_0 - 2\pi/\Lambda$, $K_{00} = K_{-1-1}$, and $K_{0-1} = K^*_{-10}$. Solving the characteristic equation (A9) for the wave velocity ω/β, and making the near stop-band assumption β_0 is approximately π/Λ, gives

$$\frac{\omega}{\beta} = V_R\frac{\pi}{\Lambda} + K_{00} \pm \sqrt{|K_{0-1}|^2} \qquad (A10)$$

Substituting the values of K_{IJ} from Appendix A1 gives the SAGW velocity expression in Eq. (40)

$$V_{\text{SAGW}} = V_R - \frac{h}{\Lambda}\frac{\rho V_R^3}{4}\left[\frac{\pi}{2}\frac{|Y_y|^2}{P_r} - \left|\frac{U_y^2}{P_r} + \frac{2U_z^2}{P_r}\right|\right] \qquad (A11)$$

APPENDIX 3

CALCULATION OF THE HEIGHT-TO-PERIOD RATIO NEEDED TO ACHIEVE A ZERO TCD FOR SURFACE ACOUSTIC GRATING WAVE PROPAGATION NORMAL TO THE X-AXIS ON ROTATED Y-CUT TRIGONAL CRYSTALS (SECTION IV.C).

The expression for the SAGW velocity was given in Eq. (40) as

$$V_{\mathrm{SAGW}} = V_R - \frac{h}{\Lambda}\frac{\rho V_R^3}{4}\left[\frac{\pi}{2}\frac{|U_y|^2}{P_r} - \left|\frac{U_y^2}{P_r} + 2\frac{U_z^2}{P_r}\right|\right] \tag{A12}$$

Assume a first order temperature variation of each of the different parameters of the form

$$X_{(T)} = X(1 + X_{TC}T) \tag{A13}$$

where

$X_{(TC)}$ is the first order temperature coefficient of the parameter

X is the parameter value at a nominal temperature (25°C)

T is the change in temperature

Making this substitution into Eq. (40), and neglecting second order temperature coefficients terms, gives

$$V_{\mathrm{SAGW}_{(T)}} = V_{\mathrm{SAGW}}(1 + V_{\mathrm{SAGW}_{TC}}T) \tag{A14}$$

where

$$V_{\mathrm{SAGW}_{TC}} = \frac{V_R V_{R_{TC}} - DD_{TC} + FF_{TC}}{V_{\mathrm{SAGW}}}$$

and

$$D = \frac{h}{\Lambda}\frac{\rho V_R^3 \pi}{8}\frac{|U_y|^2}{R_r}$$

$$D_{TC} = \rho_{TC} + h_{TC} + 3V_{R_{TC}} + 2\left(\frac{|U_y|}{P_r^{1/2}}\right)_{TC} - \Lambda_{TC}$$

$$F = \frac{h}{\Lambda}\frac{\rho V_R^3}{4}\left|\frac{U_y^2}{P_r} + 2\frac{U_z^2}{P_r}\right|$$

$$F_{TC} = \rho_{TC} + h_{TC} + 3V_{R_{TC}} + \left(\left|\frac{U_y^2}{P_r} + 2\frac{U_z^2}{P_r}\right|\right)_{TC} - \Lambda_{TC}$$

The expression for the temperature coefficient of delay is, from Eq. (41)

$$\mathrm{TCD} = \alpha - \frac{1}{V}\frac{dV}{dT}$$

Substitution of the crystal expansion coefficient in the direction of the SAGW propagation and the SAGW velocity expression found above then gives

$$\mathrm{TCD} = \Lambda_{TC} - V_{\mathrm{SAGW}_{TC}} \tag{A15}$$

Setting this TCD expression (Eq. (A15)) equal to zero, and solving for the height to period ratio gives

$$\frac{h}{\Lambda} = \frac{V_{R_{TC}} - \Lambda_{TC}}{\frac{\rho\pi V_R^2}{8}\frac{|U_y|^2}{P_r}(A_{TC}) + \frac{\rho V_R^2}{4}\left|\frac{U_y^2}{P_r} + 2\frac{U_x^2}{P_r}\right|(B_{TC})} \tag{A16}$$

This is the height-to-period ratio needed to achieve a zero TCD for a SAGW propagating normal to the X-axis on rotated Y-cut trigonal crystals (Eq. (42)).

APPENDIX 4

CALCULATION OF THE TEMPERATURE COEFFICIENT OF DELAY COMPENSATING TERM FOR SURFACE WAVE PROPAGATION UNDER THIN MASSLESS CONDUCTIVE STRIP GRATINGS (SECTION IV.F).

The temperature coefficient of delay (TCD) equation for surface acoustic wave propagation under a thin massless conducting strip grating was found to be, from Eq. (53)

$$\mathrm{TCD} = \Lambda_{TC} - V_{r_{TC}} + \frac{\Delta V_r/V_r}{2+(\Delta V_r/V_r)}\left(\frac{\Delta V_r}{V_r}\right)_{TC} \tag{A17}$$

where the unperturbed TCD term is

$$\Lambda_{TC} - V_{r_{TC}}$$

and the conducting strip perturbation temperature compensating term is

$$\frac{\Delta V_r/V_r}{2+(\Delta V_r/V_r)}\left(\frac{\Delta V_r}{V_r}\right)_{TC}$$

An expression for the temperature coefficient of the change in Rayleigh wave velocity ($(\Delta V_r/V_r)_{TC}$) can be found from the Ingebrigtsen formula (Reference 43).

$$\left(\frac{\Delta V_r}{V_r}\right) = -\omega(\epsilon_0 + \epsilon_p^T)\frac{|\phi_r|^2_{y=0}}{4P_r} \tag{A18}$$

Making the near stop band assumption

$$\omega = \frac{\pi V_r}{\Lambda}$$

gives

$$\frac{\Delta V_r}{V_r} = -\frac{\pi V_r(\epsilon_0 + \epsilon_p^T)}{\Lambda}\frac{|\phi_r|^2}{4P_r} \tag{A19}$$

and assuming only first order temperature variation, as in Appendix 3 (Eq. (A13)), gives

$$\left[\frac{\Delta V_r}{V_r}\right]_{(T)} = \frac{\Delta V_r}{V_r}\left(1 + \left(\frac{\Delta V_r}{V_r}\right)_{TC} T\right) \tag{A20}$$

In the equation above, the first order temperature coefficient term is

$$\left(\frac{\Delta V_r}{V_r}\right)_{TC} = V_{rTC} - \Lambda_{TC} + \epsilon_{eff_{TC}} + 2\left(\left|\frac{\phi_r}{P_r^{1/2}}\right|\right)_{TC}$$

where

$$\epsilon_{eff_{TC}} \approx \frac{\epsilon_{yy_{TC}} + \epsilon_{zz_{TC}}}{2}$$

$$\epsilon_{yy_{TC}} = \epsilon_{33_{TC}} \sin\theta + \epsilon_{11_{TC}} \cos\theta$$

$$\epsilon_{zz_{TC}} = \epsilon_{33_{TC}} \cos\theta - \epsilon_{11_{TC}} \sin\theta$$

θ is the rotated Y-cut angle which is 20°
for 70° X-axis cylinder.

Substituting the following numerical values

$$\frac{\Delta V}{V} = 0.02747 \text{ Slobodnik (70° } X\text{-axis cylinder)}$$

$$V_{rTC} = -0.875 \times 10^{-4}/°C \text{ Webster SAW data (70° } X\text{-axis cylinder)}$$

$$\left(\frac{\phi_r}{P_r^{1/2}}\right)_{TC} = -3.694 \times 10^{-4}/°C \text{ Webster SAW data (70° } X\text{-axis cylinder)}$$

$$\epsilon^T_{11_{TC}} = 3.82 \times 10^{-4} \text{ Smith and Welsh}$$

$$\epsilon^T_{33_{TC}} = 6.71 \times 10^{-4} \text{ Smith and Welsh}$$

$$\Lambda_{TC} = 0.154 \times 10^{-4} \text{ Smith and Welsh}$$

gives a compensation factor

$$\frac{\Delta V_r/V_r}{2 + (\Delta V_r/V_r)}\left(\frac{\Delta V_r}{V_r}\right)_{TC} = -4 \text{ ppm}$$

END

1-87

DTIC